Radio Frequency Interference and Risk of Damage For Satellite Servicing Missions

by

Jonathan D. Schiller

Submitted to the Department of Aeronautics and Astronautics
in partial fulfillment of the requirements for the degree of

Master of Science in Aeronautics and Astronautics

at the

MASSACHUSETTS INSTITUTE OF TECHNOLOGY

June 2019

Signature redacted

Author .....
Department of Aeronautics and Astronautics
May 23, 2019

Signature redacted

Certified by .....
Kerri Cahoy
Associate Professor of Aeronautics and Astronautics
Thesis Supervisor

Signature redacted

Accepted by .....
Sertac Karaman
Associate Professor of Aeronautics and Astronautics
Chair, Graduate Program Committee

Radio Frequency Interference and Risk of Damage For Satellite Servicing Missions

by

Jonathan D. Schiller

Submitted to the Department of Aeronautics and Astronautics
on May 23, 2019, in partial fulfillment of the
requirements for the degree of
Master of Science in Aeronautics and Astronautics

Abstract

This thesis assesses the potential for radiation transmitted from a servicing satellite in geostationary orbit to couple into the receivers on its intended client, thereby causing interference or even damage to receiver components. It begins by examining the satellite servicing paradigm, and introducing as case studies two missions that are currently in development. Then the theory of coupling is presented, starting with an overview of antennas, working toward the Friis transmission formula, and adapting it to be valid in the near-field. The analysis tools used are described, including TICRA GRASP, antenna modeling software used to apply the theory to this specific case. In GRASP, models of two servicing satellites representing Northrop Grumman's Mission Extension Vehicle (MEV) and DARPA's Robotic Servicing of Geosynchronous Satellites (RSGS) programs are created, as well as a model of a generic communications satellite to serve as their client. Two different communications systems are examined, with one using Ku-band and the other using both Ku-band and C-band, to see how much energy they couple into the client. The coupling is calculated over a range of distances and angles to investigate how these and other factors affected the levels seen by the receivers. Finally, the received levels are compared with the typical environment levels of radiation expected to be seen at geostationary orbit and with the specifications of typical hardware components to determine if signal reception would be affected and if the components were being exposed to higher input power than they were rated for. This analysis finds that during proximity operations, coupling can often rise above levels that would interfere with client operations and potentially damage some components, most critically the Low Noise Amplifier. In most cases, these risks occur when the servicer is closer than 100 m and directly above or below the client, and one satellite is therefore in the main transmit beam of the other. However, depending on the architecture of the receiver, it could have proper filters in place that would attenuate coupling from a servicer down to acceptable levels. The thesis ends with a list of recommendations for actions that can be taken by servicing satellite operators and future satellite manufacturers to reduce the effects of unwanted coupling during servicing operations.

Thesis Supervisor: Kerri Cahoy
Title: Associate Professor of Aeronautics and Astronautics

Acknowledgments

There are so many people who deserve thanks for their help in this endeavor. First of all, I wish to thank the amazing faculty in the Astronautical Engineering and Physics departments at the United States Air Force Academy for their help to getting me to this point in my life. My family and friends are also deserving of much gratitude for their support along the way.

I would also like to thank Col. (ret) John Kuconis for his leadership of the Military Fellows program at MIT Lincoln Laboratory, without which I and many others would not have been able to attend graduate school in the first place. Also instrumental was Dr. Michele Schuman, for her leadership and for taking me into her group and giving me guidance on this project. There were countless staff at Lincoln Laboratory and faculty in the MIT AeroAstro department who guided me on this project with their expertise and knowledge.

I would like to give a special acknowledgment to the two main individuals who really made this all possible for me. The first, Ryan Shoup, met with me weekly and gave me invaluable guidance and feedback on my progress, even though it was not his main job at Lincoln Lab. The other, Kerri Cahoy, advised me at MIT, helped with the admissions process, made time for me in her incredibly busy schedule, gave me direction on this thesis, and educated me with her unrivaled breadth and depth of knowledge. Without any of these people, I could not hope to be where I am today, or go where I am going tomorrow.

Contents

List of Figures

List of Tables

Acronyms

CAD Computer Aided Design.

CONOPS Concept of Operations.

CPU Central Processing Unit.

CSA Canadian Space Agency.

DARPA Daefense Advanced Research Projects Agency.

dB decibel.

DOF Degree of Freedom.

ETS-VII Engineering Test Satellite VII.

FCC Federal Communications Commission.

FREND Front-end Robotics Enabling Near-term Demonstration.

GEO Geosynchronous Earth Orbit.

GO Geometrical Optics.

GTD Geometrical Theory of Diffraction.

IR Infrared.

ISS International Space Station.

JAXA Japan Aerospace Exploration Agency.

kbps kilobit per second.

LAE Liquid Apogee Engine.

LEO Low Earth Orbit.

LHCP Left Hand Circularly Polarized.

LIDAR Light Detection and Ranging.

LNA Low Noise Amplifier.

Mbps megabit per second.

MEV Mission Extension Vehicle.

MLI Multi-Layer Insulation.

MOC Mission Operations Center.

MoM Method of Moments.

NASA National Aeronautics and Space Administration.

NASDA National Space Development Agency.

NFOV Narrow Field of View.

NRL Naval Research Laboratory.

ORU On-orbit Replaceable Unit.

PO Physical Optics.

PTD Physical Theory of Diffraction.

RF Radio Frequency.

RHCP Right Hand Circularly Polarized.

RPO Rendezvous and Proximity Operations.

RSGS Robotic Servicing of Geosynchronous Satellites.

RSV Robotic Servicing Vehicle.

SNR Signal to Noise Ratio.

SSL Space Systems Loral.

STK Systems Tool Kit.

TCR Telemetry, Command, and Ranging.

TDRSS Tracking and Data Relay Satellite System.

TT&C Tracking, Telemetry, and Commanding.

WFOV Wide Field of View.

Chapter 1

Introduction

Servicing satellites on orbit has long been a dream of the space engineering and operations fields. Since the dawn of the space age, satellite operators have been limited by the designs of their spacecraft. Satellites large and small are designed with a certain mission lifetime in mind, and even if they exceed that lifetime, within a few years they are still relegated to being nothing more than space debris if they are not deorbited entirely. They are also limited by a myriad of other factors as well. For example, the size of a standard payload fairing on a launch vehicle limits spacecraft size, while the amount of propellant on the launch vehicle limits its launch mass. Both of these constraints impose further limits on spacecraft design: there can only be a certain amount of fuel on board before it gets too heavy, the antennas and solar arrays can only be so large before they cannot fit inside the fairing, etc. An iterative approach addresses the constraints and the cycle keeps going until a solution is found that meets mission requirements.

On orbit servicing promises to alleviate some of these problems. It will not solve everything, since all launch vehicle payload fairings still have the same maximum size and spacecraft still must fit comfortably within these boundaries. However, having a satellite that can perform modifications and repairs on other satellites can greatly expand the length and scope of missions by replenishing fuel tanks when they run low, installing upgrades or repairs such as additional solar arrays or modular payloads, or relocating a satellite from one orbit to another. It could potentially even rescue a

mission from failure by diagnosing and correcting anomalies.

Reaching the point where servicing can be done requires numerous technological developments and demonstrations. This includes several precursor missions to validate the technology that would be required. The following are a few of the precursor missions that have been flown:

- Engineering Test Satellite VII (ETS-VII) was a mission launched in late 1997 by the National Space Development Agency (NASDA), now the Japan Aerospace Exploration Agency (JAXA). It included a large "chaser" satellite equipped with a 6 Degree of Freedom (DOF) robotic arm and a smaller "target" satellite launched together as a pair, which were capable of docking and undocking from each other. The main experiments performed included tests of docking both autonomously and with operator control; separating the chaser and target by up to 15 km and then performing rendezvous and docking procedures; and smaller experiments including machine vision processing analysis, manipulation of tools, grappling of structures, vibration analysis, and on orbit assembly of an antenna. Communications with the ground were done via an S-band single access high gain antenna, with data relayed through the National Aeronautics and Space Administration (NASA) Tracking and Data Relay Satellite System (TDRSS). Communication between the chaser and target was handled with a unified S-band link that was the target's only method of communication. The S-band link also served as a backup for the chaser. [10]

- Orbital Express was a 2007 mission by the Daefense Advanced Research Projects Agency (DARPA). It consisted of a servicer satellite called ASTRO, also with a six DOF robotic arm, and a target satellite called NEXTSat. The pair were launched together and tested technologies necessary for satellite servicing such as Rendezvous and Proximity Operations (RPO), capture and docking using ASTRO's robotic arm, fluid transfer between satellites, and installation of an On-orbit Replaceable Unit (ORU), in this case, a battery. Multiple capture tests were done with NEXTSat static and free flying. The fluid transferred between

the two satellites was hydrazine, done to demonstrate the viability of refueling satellites that rely on monopropellant for propulsion and stationkeeping. The ORU installation was intended to demonstrate the viability of installing upgrades to satellites once already on orbit. Operations were increasingly autonomous as the mission went on; the first ORU transfer completed was done with operators approving each and every step from the ground, while the last one was completely autonomous, with operators only needing to give approval to begin the installation. [18]

- The Robotic Refueling Mission was a joint venture between NASA and the Canadian Space Agency (CSA) that launched a module and four specialized tools to the International Space Station (ISS). [19] Using the ISS's robotic arm, operators on the ground used the tools to perform tasks such as peeling back Multi-Layer Insulation (MLI), unscrewing screws, opening and closing valves, making electrical connections, and transferring fluids. This was the first demonstration of a fluid transfer to or from a space vehicle that was not specifically designed to be serviced, demonstrating that satellites currently in orbit could be refueled without any need for modification. [21] A follow up to the initial mission in 2015 tested necessary technology and procedures for coolant transfer, machine vision technologies, a tool to validate correct electrical connections, and an experimental solar cell. [20] A second 2018 follow up mission intends to demonstrate the feasibility of the transfer of cryogenic fluids. [23]

These missions served to establish the basic principles and develop the underlying technology behind satellite servicing. Now, with the addressable market for satellite servicing estimated to reach as much as $3 billion, several private companies and government agencies are vying to be the first to provide robotic servicing on orbit to commercial and government customers. Projects underway include the Mission Extension Vehicle (MEV), a project of Orbital ATK (now a part of Northrop Grumman), the Robotic Servicing of Geosynchronous Satellites (RSGS) program, a program of the DARPA Tactical Technology Office, and Restore-L, a NASA project focused on

servicing satellites in Low Earth Orbit (LEO). [22] This thesis focuses on the servicing of satellites in Geosynchronous Earth Orbit (GEO), and therefore focuses on the Mission Extension Vehicle (MEV) and Robotic Servicing of Geosynchronous Satellites (RSGS) programs.

1.1 Satellite Servicing in Geostationary Orbit

Geostationary orbit, commonly called the "GEO belt," is 35,786 km above the Earth's equator. It is notable because its orbital period is exactly one sidereal day, meaning that a satellite placed in this orbit remains over the same geographical point on the Earth absent any orbital perturbations. This property comes with a great deal of benefits, and has caused the GEO belt to become populated with many billions of dollars worth of commercial and government satellites performing a variety of missions. Communications satellites can be placed there to cover entire continents without having to move antennas in space or on the ground. Weather satellites can collect atmospheric data about a particular region and be dedicated to that part of the world. Spy satellites can keep a 24/7 watch anywhere between 60°S and 60°N.

Between 1996 and 2014, there were at least 139 reported anomalies from geostationary satellites. [11, 16] While some were minor and temporary, others were much more severe and led to the loss of the entire mission. Common anomalies include power system failures, processor failures, temporary and complete loss of attitude control, single event upsets, and deployment issues. Once on orbit, there is little that can be done to correct certain types of anomalies, and this can lead to mission lifetimes being cut short by years, causing potentially billions of dollars in lost revenue for a corporation or degraded capabilities for a government agency. Because of the high value nature of these satellites, and the added benefit of them all residing at the same orbital altitude and inclination, a business case is able to be developed for a servicing satellite in GEO. Such a satellite would be well-equipped to solve many of the problems that commonly occur with geostationary satellites. Below is a selected list of just a few missions which experienced anomalies that could have been addressed

by a servicer, had one been available:

- Between 2002 and 2003, Echostar VIII lost 3 of the 12 thrusters it used for attitude control and stationkeeping. While this did not critically impact the mission, it led to inefficient use of propellant and put a greater degree of wear on the other thrusters as well as some of the gyros. A servicing satellite could potentially have refueled the satellite to make up for greater fuel expenditures, taken over attitude and stationkeeping for Echostar VIII, or even repaired the thrusters if possible. [16]

- The xenon propulsion system on Satmex V failed unexpectedly, causing the mission to resort to its backup bi-propellant propulsion system. This reduced the mission life by more than one year. A servicer could have replenished some bi-propellant in the backup propulsion system to extend the service life of the satellite, it could have taken over the propulsion duties from its client, or it could have attempted to repair the primary xenon propulsion system. [16]

- In 2005 JCSAT-1B lost control of its attitude and had to be replaced with an on-orbit spare. The anomaly has been attributed to a faulty thruster. A servicing satellite could have performed a maneuver to regain control of JCSAT-1B's attitude, assuming that the faulty thruster could be commanded off, and provided propulsion on its behalf afterward. [16]

- The north solar array on Telstar 14R did not deploy properly, leading to lower power generation and a shorter mission lifetime. The anomaly was due a clip coming loose and the solar array getting caught in wiring which was supposed to be contained by this clip. A servicer would have been able to move the wires and the clip into their desired positions, allowing the solar array to deploy fully and the mission to go on as planned. [16]

As demonstrated by the above missions and their reasons for failure, a servicing satellite could help mitigate issues in a variety of ways. It can either take over the attitude control and stationkeeping responsibilities from its client, or it can repair the

faulty parts on the client which prevent it from performing these functions on its own. These two approaches to servicing represent two schools of thought when it comes to servicing satellites in the GEO belt; the former is a more conservative approach that requires a servicer dedicated to its client for a long period of time, while the latter is a more complex approach that can perform more servicing operations in its lifetime, but also must be vastly more capable in order to deal with a wide variety of anomalies and have enough propulsion to visit multiple satellites. The more conservative approach is represented by the MEV program, while less conservative approach is represented by the RSGS program. These two programs are explained in greater detail below.

1.2 Current Satellite Servicing Programs

1.2.1 Mission Extension Vehicle

Background

The Mission Extension Vehicle is a project of Space Logistics, LLC, a subsidiary of Northrop Grumman specifically focused on satellite servicing and in-space robotics. It aims to provide mission extension services in GEO to include client satellite inspection, assuming attitude control functions, stationkeeping, and relocation to different orbital slots. It will accomplish this by rendezvousing and docking with a client satellite to form a "stack," after which the client will continue to perform all normal functions while the MEV handles all of the attitude control and propulsion needs for the en-

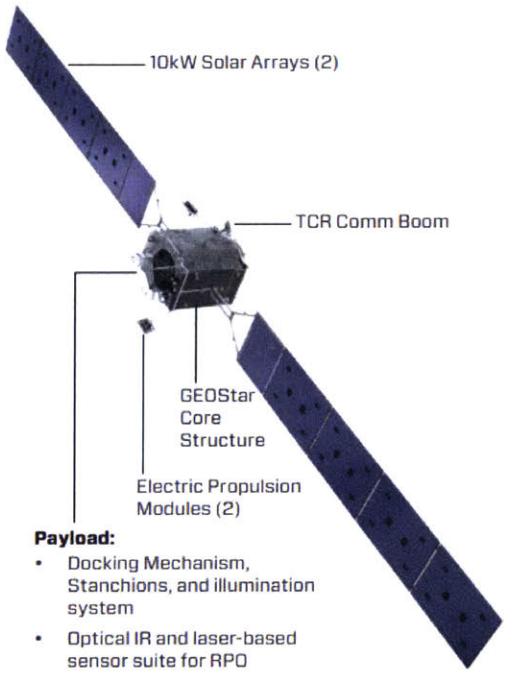

Figure 1-1: A diagram of MEV-1 from a Northrop Grumman fact sheet

tire stack. The first iteration of this program, MEV-1, is slated for launch in mid-2019 [9] and is contracted to extend the life of Intelsat 901 by five years, although MEV-1 itself is designed for a mission life of 15 years. Intelsat has also contracted with Northrop Grumman to purchase the mission extension services of MEV-2, though a specific client satellite has not yet been selected. [12]

CONOPS

As MEV-1 will serve as a demonstration mission, it will first launch into the GEO graveyard orbit, about 300 km above geostationary orbit. It will dock with Intelsat 901 there instead of its original orbital slot to avoid disturbing operations in the GEO belt and to mitigate the effects of any anomalies that might occur. MEV-1 will be equipped with a suite of RPO sensors, to include a Wide Field of View (WFOV) and a Narrow Field of View (NFOV) camera in both the visible and Infrared (IR) spectra to determine position and attitude relative to the client, a Light Detection and Ranging (LIDAR) module to provide high resolution ranging and attitude information, lighting to illuminate the client spacecraft where MEV-1 is to make contact, and both an on board and ground-based image processing suite. These sensors are used in combination with ground based measurements to obtain relative position and velocity of MEV-1 compared to its client and help in planning maneuvers on approach. Once MEV-1 gets within Intelsat 901's stationkeeping box, it will begin a series of autonomous maneuvers to approach its client, stopping at certain predetermined points along the way to ensure safety of the procedure and mitigate anomalies should they occur. MEV-1 will approach Intelsat 901 from above, and will deploy an extendable mechanism to grapple its Liquid Apogee Engine (LAE) that will retract after it makes contact, pulling the two satellites together to form the final stack. In the case of Intelsat 901, MEV-1 will then transport it to a new orbital slot for a period of five years. The entire time, MEV-1 will be affixed to the "back" of Intelsat 901, opposite from the Earth and the direction of its service beams.

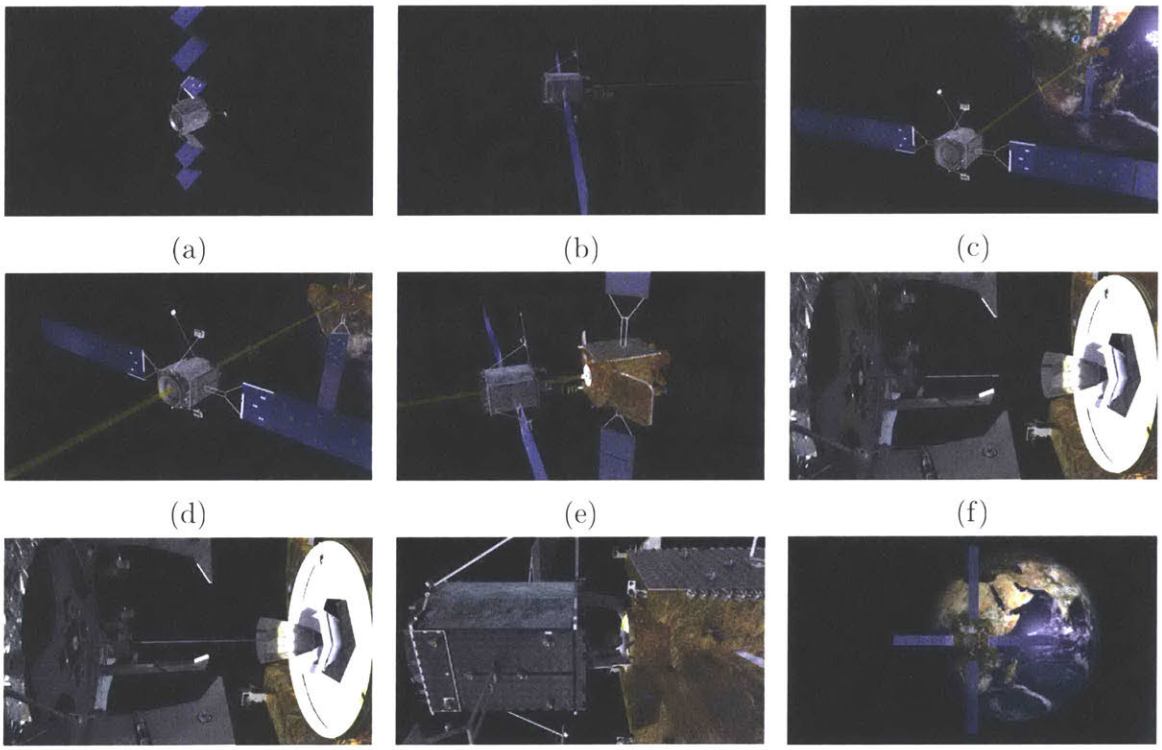

Figure 1-2: MEV-1 Concept of Operations (CONOPS): (a) MEV-1 performs checkouts and boosts itself to GEO graveyard orbit. (b) MEV-1 maneuvers to place itself directly above client. (c) MEV-1 begins to approach client from above starting at approximately 80 m. (d) MEV-1 continues to approach, holding again at 20 m above client. (e) MEV-1 continues the approach, this time getting withing 1 m of client. (f) MEV-1 releases a mechanism to grapple with the client once it is in range. (g) The mechanism attaches to the inside of the client's LAE and retracts to pull the two satellites together (h) Tension on the mechanism keeps MEV-1's stanchions firmly pressed against the client's launch adapter ring. (g) MEV-1 maneuvers the 2 satellite stack around, performing attitude control and stationkeeping for both. [4]

Communication Architecture

The communications technology being employed on MEV-1 is proprietary, but publicly disclosed information gives some clues to how it works. As seen in 1-1, the MEV comes equipped with a Telemetry, Command, and Ranging (TCR) boom. In its Federal Communications Commission (FCC) filings, Space Logistics says that MEV-1 will have only a Tracking, Telemetry, and Commanding (TT&C) link, to include one low rate Ku-band transmit antenna that operates between 11.45 GHz and 12.25 GHz and two C-band transmit antennas that can be operated at a low (4.8 kilobit per second (kbps)), medium (18 kbps), or high (1 megabit per second (Mbps)) data rate in the band between 3.7 GHz and 4.2 GHz. There will also be matching receive antennas in Ku-band (13.75-14.5 GHz) and C-band(5.925-6.425 GHz). It is presumed that they will be located on this TCR boom. All antennas will be hemispherical antennas, abbreviated HEMI in documentation, that have one wide main lobe pointed in the general direction of the Earth. FCC filings include link budgets for all of these antennas, for both uplink and downlink. [28]

1.2.2 Robotic Servicing of Geosynchronous Satellites

Background

The RSGS program began as an idea from DARPA, who then presented it to industry groups in order to form a public-private partnership to develop the spacecraft. The idea was that DARPA would provide some funding, a launch vehicle, logistics, and a payload while a private company would develop the spacecraft bus and integrate the payload on it. [24] DARPA would choose the first client to be serviced to validate the functionality, and then their industry partner would assume all operations to provide commercial servicing to customers in the GEO belt. The payload to be provided was a suite of tools and two robotic arms based on the Front-end Robotics Enabling Near-term Demonstration (FREND) robotic arm developed by the Naval Research Laboratory (NRL). With these arms, the Robotic Servicing Vehicle (RSV), the satellite produced by the RSGS program, would be able to grab onto a client

satellite and either perform maneuvers to change its orbit or manipulate components on the client to repair mechanical anomalies, install upgrade packages, or even replenish spent propellant. The suite of tools on board are all designed to interface with the FREND arms and be changed out depending on which tool is needed for a given task. The payload also includes WFOV and NFOV imagers as well as a LIDAR module to perform inspections of a client before approaching. [24]

In February 2017, DARPA announced that it was choosing Space Systems Loral (SSL) as its partner. [6] As such, SSL began developing the RSV bus, to be later integrated with the payload. Four months later, it was announced that communications satellite operator SES had agreed to be the first customer for RSGS services, although a specific client satellite was not named. [13] However, in January 2019, after reevaluating its financial position, SSL decided to cancel its contract with DARPA to build the RSGS bus. DARPA is currently considering its options to determine whether it will try to hold another competition for bids to construct the bus. Its intention, however, is to move the program forward. [14]

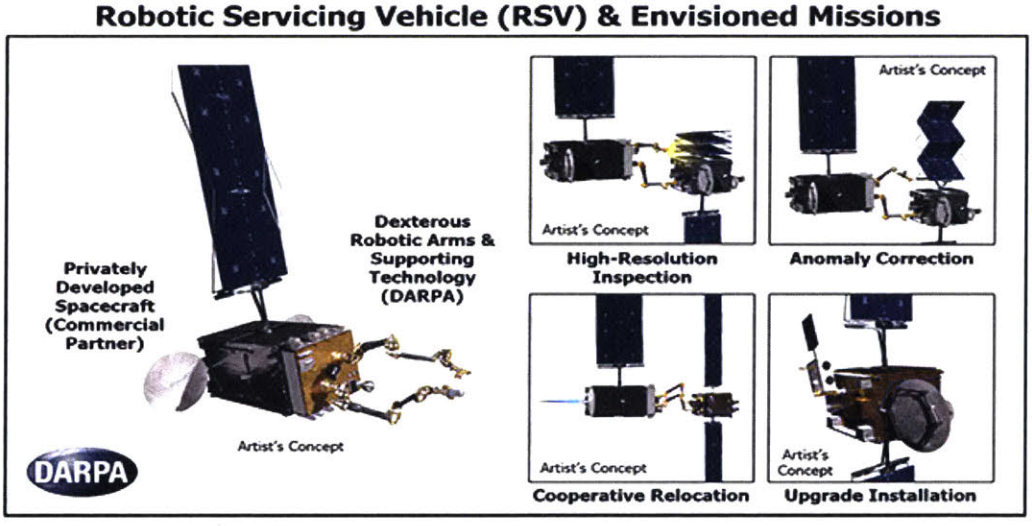

Figure 1-3: Artist's concept of the RSGS program's RSV, as well as some of the capabilities it is designed to have.

1.2.3 CONOPS

The RSV will be launched into a geostationary transfer orbit, from which it will boost itself into GEO. Then it will perform checkouts to make sure all systems are operating nominally. Once ready to begin servicing its first client, it will perform a rendezvous maneuver to move itself to its client's orbital slot. Before it approaches, it will spend several weeks performing RPO with the client, inspecting it with its cameras and LIDAR to form a 3D model of the client it can then use to plan its interactions. Once it has this model, it will approach and grapple with the client using one of the FREND arms. from that point, it can use the other arm to make repairs, install self-contained additional payloads, replenish expendables or various other servicing tasks, or it can also maneuver the pair of satellites to another orbital slot or to the GEO graveyard orbit. Once it is done servicing a given client, it will boost itself into the GEO graveyard orbit to rendezvous with its next customer, or wait until it is needed if one has not yet been identified. [24]

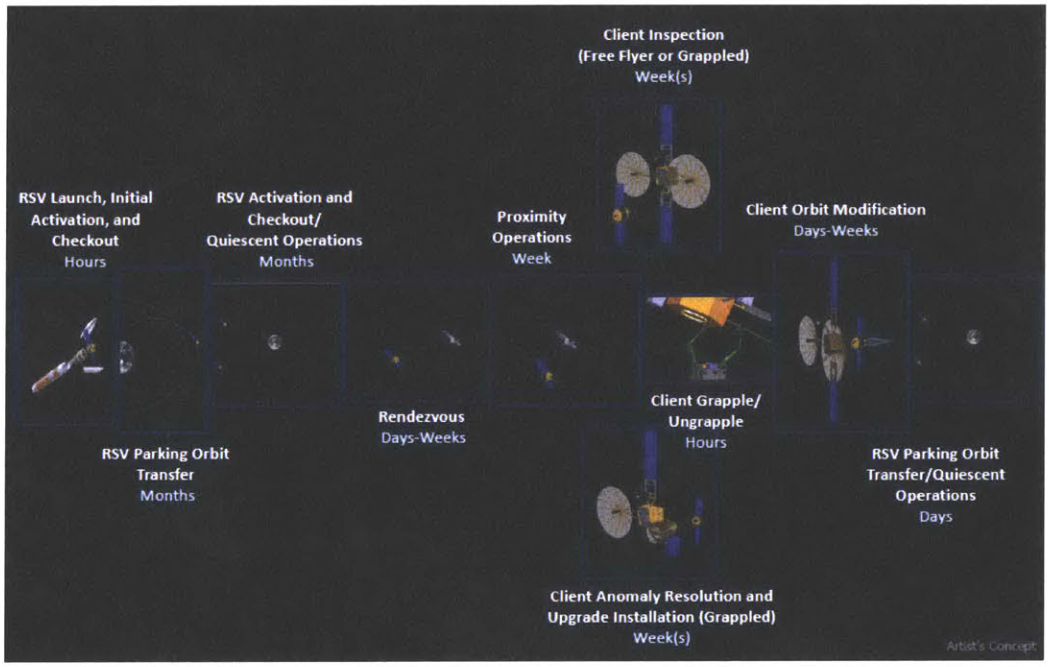

Figure 1-4: The Concept of Operations for RSGS as envisioned by DARPA

Communication Architecture

The communications subsystem for RSGS had not been finalized before the cancellation of the contract between SSL and DARPA. Now that the contract has been terminated, the design of the subsystem is even more uncertain, but there are some indications of intentions from DARPA. First, they have stated that they want to have an uplink data rate of at least 10 kbps and a downlink data rate of at least 10 Mbps to accommodate live video feeds of relevant servicing actions as well as all necessary telemetry. This requires a system that can handle these kinds of data rates. DARPA has stated that they are using Radio Frequency (RF) communication as a baseline for the RSV, likely in Ku-band, and this is what the data rate requirements assume. Optical communications are also under consideration, but are not considered to be part of the baseline. [26] This thesis assumes that the eventual RSGS contractor follows through on plans to build an RF communication system in Ku-band. Beyond this there exists very little public detail about plans for this system, however most artists' depictions show the RSV having two parabolic reflector antennas on opposite sides of the spacecraft bus (see Figure 1-3), and since this provides a sufficiently different solution than that used by the MEV program, this type of architecture is investigated further.

1.2.4 The Problem: RF Coupling

There are a great deal of challenges in servicing satellites. Not a single satellite currently in orbit was designed with servicing in mind, and so design choices that could have made servicing easier, such as adding a refueling port, for example, are not yet made. But the issue goes even beyond that. Most satellites, including large, multi-billion dollar geostationary satellites, are not designed to have other satellites in close proximity to them. The RF chain of the receivers on most satellites are designed to isolate and reject their own RF transmit signal, but they could not have reasonably planned on having another satellite broadcasting on similar frequencies at high enough power to close a link between Earth and GEO.

This presents a problem for those who wish to service other satellites. If an RF communication system is used, some of the energy from the servicer's transmitter will couple into the client's receiver. Likewise, the servicer also has to be wary of energy from the client's transmitters coupling into its receiver. The amount of energy that is coupled between one satellite and the other is the key here; low levels may be negligible, higher levels may cause interference that is unacceptable to a communication satellite operator trying to maintain uninterrupted service, and still higher levels may exceed the operational maximum input power of components in the client's receiver and damage them irreparably. It is important to model the way RF energy interacts between two satellites and to see just how much energy is coupled between them to determine the level of risk to both the servicer and the client.

This thesis attempts to answer the question of how much RF energy couples into the client and servicer receivers and whether or not these levels are detrimental to one or both missions. Chapter 2 introduces the theory of coupling as well as TICRA GRASP, the tool used to calculate it. Chapter 3 discusses the modeling that is done to ensure realistic results and the validation of these models, and then goes into the design for the specific scenarios run in GRASP to determine levels of coupling. Chapter 4 explores the results of these scenarios and presents the peak coupling values seen in each of them. Chapter 5 draws conclusions from the results of simulations of both spacecraft and makes recommendations for how to safely communicate during servicing operations.

Chapter 2

Background

This chapter discusses the theory of RF coupling introducing a framework necessary for this analysis, starting with the basics of how antennas radiate to a more robust treatment of how antennas couple energy, taking into account aspects such as transmit power and phase. It also gives an overview of the tool used to compute coupling for this thesis, TICRA GRASP, and how it handles coupling and other calculations.

2.1 Coupling Theory

2.1.1 Antenna Basics

At its simplest, an antenna is a component with the function of radiating or receiving electromagnetic waves. It is created when a charge contained within it moves, causing an electromagnetic disturbance that travels outward at c, the speed of light. When this motion becomes oscillatory, such that charge moves back and forth within the antenna in a sinusoidal manner, the disturbance that is propagated also takes the form of a sine wave with the same frequency as the input electrical signal that created it, becoming an electromagnetic wave traveling through free space. This wave does not spread out evenly in all directions however, as it would from an electric monopole. The simplest form of antenna, a dipole antenna, can be pictured as a pair of rods aligned on a single axis, with each attached to a transmission line such that current

moves back and forth along the rods' axes in a synchronized manner. That is, current moves into one rod and out of the other so that the current in both rods is moving in the same direction at the same time so that charges move in one direction and then the other in a sinusoidal manner. This, depending on the ratio of the antenna's length to the wavelength of the wave being produced, creates lobes of radiation in a ring around the rods, with nulls at the rod's endpoints. The shape of the radiation produced is known as a radiation pattern, and this pattern can be quite different depending on the geometry of the antenna being used. [17] Many types of antennas focus much of the radiation they emit in one specific direction. This is measured by the directivity, the ratio of the amount of power radiated by an antenna in its peak direction to the amount that would be radiated by an isotropic antenna (one that radiates equally in all directions). The gain of an antenna is a measure of its directivity with losses taken into account.

Just as antennas use charge moving through a conductor to produce an oscillating electromagnetic field, they are also susceptible to oscillating electromagnetic fields moving charges around within them. This forms the basis of communication over free space with radio waves; the former situation describes a transmitter, while the latter describes a receiver. The radiation produced by one antenna creates an electric current in the other, thereby sending a signal between the two. The danger here is that the receiver picks up any signal it encounters, not necessarily only ones with the transmitted signal it is expecting. So, great care must be taken to ensure that receivers only pick up signals from the intended transmitters; in many cases filters are placed in RF receivers to attenuate undesired frequencies, as well as amplifiers that are designed for signals in a specific frequency range.

This thesis is concerned with the possibility that in the specific case of satellite servicing, existing measures to isolate the receivers on a satellite may not be enough. As shown in Section 2.1.2, receivers on geostationary satellites must be extremely sensitive in order to pick up faint signals coming toward them from Earth. They are designed so that they are isolated from the transmitters on board that satellite, but in all likelihood, their design did not factor in a second satellite transmitting in

such close proximity, with high enough power to close a link with a ground station on Earth. [25]

2.1.2 Friis Transmission Formula

The first step in determining the coupling between antennas on two satellites is to consider the simple case of two antennas pointing directly at each other at a reasonably large distance. A transmitting antenna with an input power P_t outputs that amount of power minus any losses that occur in the transmit RF chain. This power then gets directed more in some directions than others according to the antenna's radiation pattern; along an antenna's boresight, the transmitted power is given by the expression $P_t D_t$, where D_t is the antenna's directivity. The power that is emitted by the transmit antenna in the direction of the receiver goes on to propagate through free space, incurring a path loss according to the inverse square law. The power density of the radiation at any given point is given by Equation (2.1), where R represents the distance from the transmitter.

$$S = \frac{P_t D_t}{4\pi R^2} \tag{2.1}$$

This energy is then collected by a receive antenna with an effective aperture of area A_{er}. Thus, the received power is given by Equation (2.2).

$$P_r = S\varepsilon_a A_p = \frac{P_t D_t A_{er}}{4\pi R^2} \tag{2.2}$$

This solution is inelegant, however, as it requires a measure of directivity for one antenna and an aperture size and efficiency for the other. However, according to the antenna reciprocity theorem, the properties of an antenna such as directivity and effective aperture are the same whether an antenna is used for transmitting or receiving. Therefore, an alternative way of formulating Equation (2.2) is shown by Equation (2.3), where D_r is the directivity of the receiver and A_{et} is the effective

aperture of the transmitter.

$$P_r = \frac{P_t D_r A_{et}}{4\pi R^2} \tag{2.3}$$

Equations (2.2) and (2.3) can be rearranged to form the relationship shown in Equation (2.4).

$$\frac{A_{et}}{D_t} = \frac{A_{er}}{D_r} \tag{2.4}$$

If the transmitting antenna is assumed to be isotropic, then $D_t = 1$, and its aperture is equal to $\frac{A_r}{D_r}$. Since this must hold true for all receiving antennas, plugging in vales for any antenna can give the effective aperture of an isotropic antenna. The simplest such values are those from an ideal isotropic antenna, which has a directivity of $\frac{3}{2}$ and an effective aperture of $\frac{3}{8\pi}\lambda^2$. Plugging these values into Equation (2.4) gives a value of $\frac{\lambda^2}{4\pi}$, where λ is the wavelength of the wave being radiated, for the effective aperture of an isotropic antenna. Using this value, Equation (2.4) can be rearranged to form an expression for the directivity of an antenna given its aperture. [27]

$$D = \frac{4\pi}{\lambda^2} A_e \tag{2.5}$$

This directivity does not account for losses, however. A more commonly used metric is the gain, which is the directivity multiplied by an aperture efficiency ε_a, a measure of losses due to a number of factors such as amplitude tapering toward the edge of the aperture, spillover from a feed that does not get reflected off of a reflector, and minor offsets in phase or polarization across the aperture. An expression for the gain of an antenna is shown in Equation (2.6).

$$G = \frac{4\pi}{\lambda^2} \varepsilon_a A_e \tag{2.6}$$

With this definition of the gain, Equation (2.2) can be rewritten in the form of Equation (2.7). This equation is known as the Friis transmission formula, and it gives

a succinct expression for the received power using the gains of both antennas.

$$P_r = \frac{P_t G_t G_r \lambda^2}{(4\pi R)^2} \tag{2.7}$$

This equation provides an intuitive foundation for understanding how antennas communicate across large distances. It is the basis by which satellite antennas are designed, as their transmit power and gains must be enough to close a link with their ground stations on the Earth's surface. However, it alone is not enough to determine the energy coupled into a satellite's receiver by another satellite transmitting in close proximity. First of all, these satellites are both intended to be communicating with the Earth, and their antennas therefore are not communicating with each other. Furthermore, their relative orientations are variable throughout the servicing process, with each receiver seeing not the peak gain, but vast swaths of the rest of the other satellite's transmit antenna radiation pattern. A single value for the gain is not very helpful in this case, and due to the great amount of sidelobes and backlobes on the patterns of some of these antennas, the relative orientations may not even be known well enough to determine a precise value of the gain for either antenna at any given time. An additional limitation is that the antenna patterns that are calculated or measured are done so using a simplifying assumption that a receiver is far away from the transmitter. This distance dependence is explained further in the following section. [25]

2.1.3 Near and Far Fields

When calculating the radiation pattern of an antenna, one finds the electric and magnetic fields produced by current carrying elements within the antenna. Rays are then drawn from each element to the point at which the field is to be calculated, and the contributions from each element are summed to find a total electric and magnetic field at that point. For the calculation of an entire pattern, this is done for multiple points over a variety of angles. These patterns assume that whatever antenna they are communicating with is far enough away so that all of the rays

from the current elements can be considered to be parallel, simplifying many of the calculations. However, when calculating the fields at a point that is sufficiently close to the current elements, these rays can no longer be assumed to be parallel. The region where this simplifying assumption holds is called the far-field, while the region in which it breaks down is called the near-field.

Calculating fields and patterns in the far-field is attractive because they can be assumed to have no radial components; the electric field is orthogonal to the magnetic field and both are orthogonal to the direction of propagation. Waves that are inherently spherical in nature, as they are radiating from what can be considered a point source at a great distance, can be treated as plane waves when they are incident on an object in the far-field because the spherical wave has become so large that an aperture can only capture a small amount of it with a negligible amount of curvature. However, performing coupling calculations between a servicing satellite and its clients involves not only the abandonment of the strictly far-field assumption, but also a knowledge of where the far-field ends and the near-field begins.

Finding the boundary between the near-field and far-field involves drawing a red line in a naturally gray area. There is no one point where it is obvious that the near-field has ended and the far-field has begun, so an approximate boundary is used to delineate the two. The commonly used criterion to determine where the near-field ends is shown in Equation (2.8), and it is based on a binomial expansion of an equation used for calculating the distance from the end of a line of current to a test point relative to the distance from the other end of the antenna to the test point in spherical coordinates. [25] In the far-field assumption, only the first two terms of this binomial expansion are used, but the third term is considered to no longer be negligible when it exceeds one sixteenth of a wavelength. This term taking on a value of greater than one sixteenth of a wavelength indicates that waves emanating from either end of the antenna are out of phase by more than this amount and are therefore at risk of interfering destructively at the test point, leading to behavior that is much more difficult to predict accurately than if all rays can be assumed to be parallel and in phase. The area where this behavior occurs is often referred to as the

Fresnel region, while the area outside of the sphere prescribed by Equation (2.8) is called the Fraunhofer region.

$$r > \frac{2D^2}{\lambda} \tag{2.8}$$

In Equation (2.8), D is aperture diameter, λ is again the wavelength, and r is the minimum distance from the antenna to be considered to be in its far-field. In order to be considered the far-field, there are two additional conditions that must be met, namely that $r \gg D$ and $r \gg \lambda$, but these are often satisfied long before Equation (2.8) is satisfied, especially on satellites operating at frequencies above 1 GHz. Beyond this, there are different sub-regions of the near-field, where reactive and radiating fields dominate calculations. The boundary of the reactive near-field is shown in Equation (2.9), while the radiative near-field exists in the region between these two boundaries. The importance of both of these regions is that the radiation pattern within them is a function of not just the angle from the antenna boresight, but also of the distance from the antenna itself. [25]

$$r < 0.62\sqrt{\frac{D^3}{\lambda}} \tag{2.9}$$

2.1.4 Coupling in the Near Field

In the near-field, calculating the coupling between two antennas becomes more challenging. The waves radiating from the transmitter can no longer be assumed to be plane waves, and may have a radial component. Additionally, at close distances, the radiation patterns of both the transmitter and receiver can differ from their measured far-field patterns, making it difficult to determine near-field behavior based on those characteristics. The introduction of a second antenna into the picture also complicates the definition of the far-field introduced by Equation (2.8), as there are now two antennas with potentially different aperture diameters and at different orientations relative to any test point. The solution for this is to introduce a modified far-field criterion for coupling between two antennas, though it still uses the same reasoning.

This new criterion is similar to the previous one, except that it adds the aperture diameters of both antennas such that the difference in phase from one end of one antenna to the opposite end of the other shall not exceed one sixteenth of a wavelength. The revised criterion is shown below in Equation (2.10), where D_t is the diameter of the transmit antenna and D_r is the diameter of the receive antenna.

$$r > \frac{2(D_t + D_r)^2}{\lambda} \tag{2.10}$$

While calculating coupling between antennas that are in the far-field of each other can be done rather simply via Equation (2.7), it becomes much more difficult when they are closer than the distance specified in Equation (2.10). In practice, rather than characterizing a radiation pattern for every antenna at every angle at varying distances, a computational approach to near-field coupling is taken that models the aperture of the transmitting antenna as a collection of small radiating current elements that are essentially dipoles. Each of these elements is small enough that it satisfies the criterion in Equation (2.10) with the receiving antenna individually and therefore they can all be considered transmitting antennas in the far-field of the receiver. To find the coupling, the coupling contributions from each element is found and added up to produce a total coupling number. However, this alone is not enough to give an accurate picture of the coupling in a complex system containing other structures besides the two antennas. There may also be scattering off of nearby surfaces that must be considered, such as waves being reflected off of a satellite bus and into the receiver. In this case, the phase of the waves also becomes an important factor, whereas the Friis equation did not consider this at all. In order to take phase into consideration, a more complete coupling expression is required than the one given in (2.7). [15]

2.1.5 A More Refined Coupling Formulation

To account for the phase of the waves radiating from an antenna, a complex vector field $\mathbf{e}(\theta, \phi)$ is introduced to represent the pattern of the antenna. This vector pattern

has units of V/m and is oriented in the direction of the polarization of the field. At any distance r in the far-field of an antenna, the time invariant electric field produced is given by Equation (2.11). The time varying field can be found by multiplying by a factor of $e^{j\omega t}$, but this analysis focuses on only the spatial components of the field, which work out to be the peaks of the time varying field anyway.

$$\mathbf{E}(r,\theta,\phi) = \frac{e^{-jkr}}{kr}\mathbf{e}(\theta,\phi) \tag{2.11}$$

In this equation, r, θ, and ϕ are spherical coordinates with an origin at the center of the antenna aperture, $j = \sqrt{-1}$ is the imaginary unit, and k is the wave number given by $k = \frac{2\pi}{\lambda}$ or alternatively $k = \omega\sqrt{\mu\varepsilon}$ where ω is the angular frequency of the wave, μ is the permeability of the propagation medium, and ε is the permittivity of the medium. Using this definition, the magnetic field is given by Equation (2.12), where $Z = \sqrt{\frac{\mu}{\varepsilon}}$ and is the impedance of the medium.

$$\mathbf{H}(r,\theta,\phi) = \frac{1}{Z}\hat{r} \times \mathbf{E}(r,\theta,\phi) \tag{2.12}$$

The average power flux density over one full wavelength of oscillation is given by one half of the real part of the Poynting vector, shown in Equation (2.13).

$$\mathbf{S} = \frac{1}{2}\mathrm{Re}[\mathbf{E} \times \mathbf{H}^*] \tag{2.13}$$

This evaluates to the expression shown below.

$$\mathbf{S} = \frac{1}{2}\,\mathrm{Re}[\frac{e^{-jkr}}{kr}\mathbf{e}(\theta,\phi) \times \hat{r} \times \frac{e^{jkr}}{Zkr}\mathbf{e}^*(\theta,\phi)] = \frac{|e(\theta,\phi)|^2}{2Z(kr)^2}\hat{r} \tag{2.14}$$

Consequently, the gain pattern of an antenna can also be expressed by dividing the above expression by the power flux density of an isotropic point source, shown in Equation (2.15). The gain pattern expression is shown in (2.16).

$$\mathbf{S}_{iso} = \frac{P_t}{4\pi r^2} \tag{2.15}$$

$$G = \frac{\varepsilon_a \mathbf{S}}{\mathbf{S}_{iso}} = \frac{\varepsilon_a \lambda^2 |e(\theta, \phi)|^2}{2\pi Z P_t} \tag{2.16}$$

In order to use the vector field pattern to produce an expression for coupling, one must turn to the antenna reciprocity theorem, which states that the amplitude of the signal delivered to a receiver by a plane wave incident on the antenna feeding that receiver is proportional to the scalar product of the incident vector field pattern and the vector field pattern of the receiving antenna were it instead used as a transmitter. A statement of the reciprocity theorem is shown in (2.17).

$$\oint_A (\mathbf{E}_1 \times \mathbf{H}_2 - \mathbf{E}_2 \times \mathbf{H}_1) \cdot \mathbf{n} \, \mathrm{d}A = 0 \tag{2.17}$$

In this equation and the following equations, subscripts of 1 indicate a field radiated from the antenna in question while subscripts of 2 indicate a field incident on the the antenna. The integration is performed over a closed surface A, where $\mathbf{n}$ is the normal vector to A. The argument of the integral bears resemblance to two instances of a Poynting vector, however it crosses together electric and magnetic fields from two different wavefronts, a transmitting and receiving one, which may or may not exist simultaneously. Also of note is that the closed surface A includes a region on it in which waves fed through a waveguide pass through it. That is, waves either enter A through the waveguide and exit after being transmitted by the antenna, or they enter A from outside and are incident on the antenna aperture, after which they are collected and sent into the waveguide to leave A. Since waves can freely enter and exit A via one of these two routes, their contributions to the integral in Equation (2.17) are not zero, however the theorem states that they must sum to zero. By calculating each of the contributions to this integral, it can be seen exactly what the contributions to it are of the incident and transmitted waves, and therefore the relationship between them.

To find the contribution of the waveguide, the following definitions of the electric

fields are used, keeping the subscript definitions introduced above.

$$\mathbf{E}_1(x,y,z) = a\mathbf{e}_w(x,y)e^{-j\beta z} \tag{2.18a}$$

$$\mathbf{E}_2(x,y,z) = b\mathbf{e}_w(x,y)e^{+j\beta z} \tag{2.18b}$$

Here, most notably, a and b are the amplitudes of the transmitted and received signals respectively, while $\mathbf{e}_w(x,y)$ is the vector field pattern of the waveguide and β is its propagation constant. The magnetic fields associated with these electric fields are as defined in Equation (2.12). Using these field definitions, the integral in Equation (2.17) can be evaluated as follows.

$$\iint_{A_w} (\mathbf{E}_1 \times \mathbf{H}_2 - \mathbf{E}_2 \times \mathbf{H}_1) \cdot \mathbf{n}\, \mathrm{d}A = \frac{2ab}{Z} \iint_{A_w} |e_w(x,y)|^2 \,\mathrm{d}x\,\mathrm{d}y \tag{2.19}$$

Also of note is the evaluation of the Poynting vector for the transmitted wave, as the integration of this vector over a cross section of the waveguide can give an expression for the transmit power.

$$\frac{1}{2}\,\mathrm{Re}[\iint_{A_w} \mathbf{E}_1 \times \mathbf{H}^* \,\mathrm{d}x\,\mathrm{d}y] = \frac{a^2}{2Z} \iint_{A_w} |e_w(x,y)|^2 \,\mathrm{d}x\,\mathrm{d}y = P_t \tag{2.20}$$

This expression allows Equation (2.19) to be transformed into a more palatable form.

$$\iint_{A_w} (\mathbf{E}_1 \times \mathbf{H}_2 - \mathbf{E}_2 \times \mathbf{H}_1) \cdot \mathbf{n}\, \mathrm{d}A = 4P_t \frac{b}{a} \tag{2.21}$$

The contribution of the remainder of surface A, the portion outside of the waveguide, is more mathematically intensive to calculate. It begins with the definitions of the electric fields $\mathbf{E}_1$ on transmission from the antenna and $\mathbf{E}_2$ on reception. $\mathbf{E}_1$ is defined exactly the same as in Equation (2.11), while $\mathbf{E}_2$ is defined below.

$$\mathbf{E}_2(r,\theta,\phi) = \mathbf{e}_{inc} e^{jkr\,\mathbf{u}_{inc}\cdot\hat{r}} \tag{2.22}$$

Here $\mathbf{e}_{inc}$ represents the vector field pattern of the incident wave, which is traveling in the direction $-\mathbf{u}_{inc}$. Similar to above, the magnetic fields are found by plugging these electric fields into Equation (2.12). Evaluating the integral in (2.17) using these fields requires a stationary-phase approximation which is shown here, but it can be shown that the integral evaluates to the following.

$$\iint_{A_s} (\mathbf{E}_1 \times \mathbf{H}_2 - \mathbf{E}_2 \times \mathbf{H}_1) \cdot \mathbf{n} \, \mathrm{d}A = \frac{j\lambda^2}{\pi Z} \mathbf{e}_{inc} \cdot \mathbf{e}(\theta, \phi) \tag{2.23}$$

Combining the results of Equations (2.21) and (2.23) and setting them equal to zero as required by reciprocity in Equation (2.17), one can solve for $\frac{b}{a}$, the ratio of the received signal amplitude to the transmitted signal amplitude within the waveguide. This final ratio is shown below in Equation (2.24).

$$\frac{b}{a} = \frac{\lambda^2}{j4\pi Z P_t} \mathbf{e}_{inc} \cdot \mathbf{e}(\theta, \phi) \tag{2.24}$$

This equation shows explicitly the constant of proportionality referenced in the antenna reciprocity theorem, $\frac{\lambda^2}{j4\pi Z P_t}$. More importantly, it allows for a more complete coupling formula to be developed. If $\mathbf{e}_{inc}$ is defined as the electric field of an incoming wave as shown below, this can be substituted into (2.24) while specifying that the $\mathbf{e}(\theta, \phi)$ term in that equation is referencing the receiver (and adding a subscript of r to denote this, as well as a subscript of t for the transmitted wave).

$$\mathbf{e}_{inc} = \frac{e^{-jkr}}{kr} \mathbf{e}_t(\theta_t, \phi_t) \tag{2.25}$$

This gives the final form of the coupling equation:

$$\frac{b_r}{a_t} = \frac{\lambda^2}{j4\pi Z P_t} \frac{e^{-jkr}}{kr} \mathbf{e}_t(\theta_t, \phi_t) \cdot \mathbf{e}_r(\theta_r, \phi_r) \tag{2.26}$$

It is this form of the coupling equation that is used in this analysis, rather than the Friis version.[8]

2.1.6 GRASP Coupling Equations

The above coupling formulation is what GRASP uses when it runs a coupling analysis, with some slight modifications. In GRASP, electric and magnetic fields are normalized such that physical constants are built into the field values and therefore are not needed in calculations, where their potentially large or small values might cause computational problems. These normalizations are shown below.

$$\mathbf{E}_G = \frac{1}{k\sqrt{2Z}}\mathbf{E}_{SI} \tag{2.27a}$$

$$\mathbf{H}_G = \frac{1}{k}\sqrt{\frac{Z}{2}}\mathbf{H}_{SI} \tag{2.27b}$$

In Equations (2.27a) and (2.27b), a subscript of SI represents the $\mathbf{E}$ and $\mathbf{H}$ fields as measured in SI units and a subscript of G represents the fields as measured in "GRASP units." As k in this case has units of m^{-1} and Z has units of Ohms, both of these fields work out to have units of $\mathrm{W}^{1/2}$.

In Equation (2.26), both $\mathbf{e}_t(\theta_t, \phi_t)$ and $\mathbf{e}_r(\theta_r, \phi_r)$ are considered to be far-field electric fields, but GRASP calculates these fields at specific distances and angles, requiring it to be altered to accommodate the near-field $\mathbf{E}$ fields. Incorporating the normalization constant from Equation (2.27a) and referencing Equation (2.11) for the relation between near-field and far-field, the following equation is used to replace both the transmitted and received far-fields from Equation (2.26).

$$\mathbf{E}(r, \theta, \phi) = \frac{1}{k\sqrt{2Z}}\frac{e^{-jkr}}{kr}\mathbf{e}(\theta, \phi) \tag{2.28}$$

Finally, unless otherwise specified, GRASP assumes all transmit powers to be normalized to a value of 4π Watts. Making the substitution of Equation (2.28) into Equation (2.26) and setting P_t equal to 4π gives the following equation.

$$c = \frac{b_r}{a_t} = -\frac{1}{2}jkre^{jkr}\mathbf{E}_t(r, \theta_t, \phi_t) \cdot \mathbf{E}_r(r, \theta_r, \phi_r) \tag{2.29}$$

This is the final form of the coupling equation the is used by GRASP, and is used to evaluate how servicing satellites interact with their clients in the RF spectrum. As the fields $\mathbf{E}_t$ and $\mathbf{E}_r$ in this context both have units of $W^{1/2}$, the final value c has units of Watts. This value can be converted into decibels referenced to a value of 1 Watt (dBW) by applying the following transformation.

$$C_{dB} = 20 \log_{10} |c| \tag{2.30}$$

The absolute value is necessary because the coupling coefficient found by (2.29) is complex. It is in the form above that all coupling values are reported. [15]

2.2 The Tool: TICRA GRASP

The tool used to analyze RF coupling in a satellite servicing scenario is an antenna modeling software called GRASP, made by TICRA. [15] GRASP allows users to model antennas and additional scattering structures and analyze the radiation that is emitted from these systems. It offers analyses using Physical Optics (PO), Geometrical Optics (GO), their extensions the Physical Theory of Diffraction (PTD) and Geometrical Theory of Diffraction (GTD). It also has add-ons for additional types of analysis such as the Method of Moments (MoM) or the one utilized in this case, coupling. Its most common use is among industry professionals trying to characterize antennas being built for a variety of applications. GRASP was chosen for this project over other antenna modeling tools because of its focus on electrically large objects, its treatment of antennas and scatterers as a system rather than antennas being isolated, and its ability to consider multiple sources of radiation all at once. These factors, in addition to the presence of an add-on devoted specifically to coupling calculations, made this program the right fit for considering RF interactions between satellites.

2.2.1 The GRASP Layout

The GRASP user interface is laid out into four windows: Objects, Commands, Jobs, and Results.

In the first window, shown below, the user can place any number of objects such as antennas, feeds, plates, struts, and more into a 3D environment defined by one or more coordinate systems, which can be defined relative to other coordinate systems, creating a hierarchy. Defining components in different coordinate systems allows the user to analyze different configurations and/or orientations of a given system, and move a group of objects all defined in the same or child coordinate systems all at once rather than individually. This feature becomes very important later on.

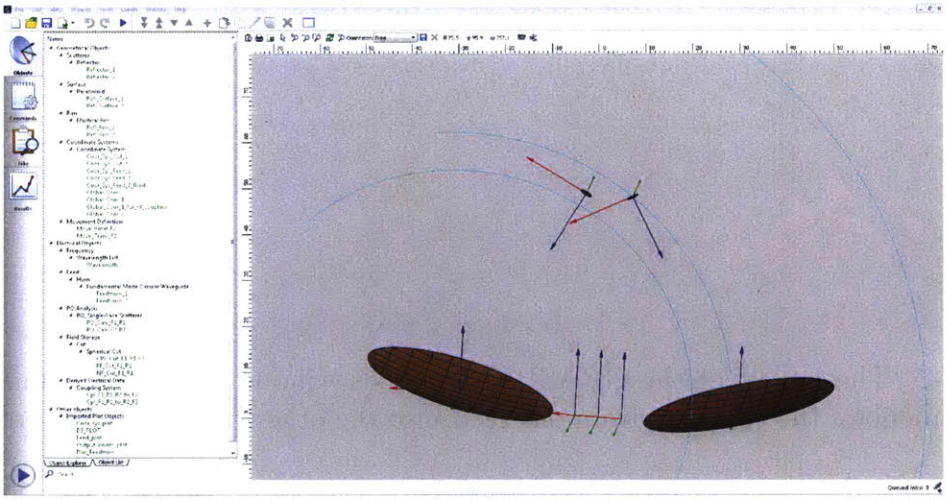

Figure 2-1: The layout of the Objects window in GRASP, showing a tutorial coupling example with two parabolic reflectors and their feeds in the near field of each other.

The second window lists the commands used to generate the output desired by the user. They can differ based on the type of analysis being run, but there are several key commands that are frequently used. The "Get Currents" command allows the user to select multiple sources of radiation and one target on which to calculate the surface currents produced by the fields from each of the sources. Once currents have been calculated on a surface, whether a reflector or a scatterer, that surface can then be used as a source to calculate the currents on a subsequent surface. The "Get Field" command allows the user to find the radiation pattern of an antenna or

for any surface which has had its currents calculated. Additionally, the "Add Field" and "Subtract Field" commands allow users to calculate the radiation pattern from one source, and then modify it with field contributions from other sources, allowing them to model more complex antenna structures and systems that consist of more than just a single transmitting antenna. Somewhat more relevant to this project, the "Get Coupling" command calculates the coupling between one or multiple sources (antennas or surfaces which have had currents calculated) and an antenna or feed that acts as the receiver. An example Commands window is shown below.

Figure 2-2: The layout of the GRASP Commands window, with commands shown used to calculate the coupling from one feed into the other by way of both reflectors.

The Jobs window lists all jobs that are currently running or that have completed running in a given project. A "job" in this context is when GRASP takes the objects as defined in the Objects window and runs through each of the commands in the Commands window sequentially to produce an output. The list of present and past jobs is displayed on the left, while the window on the right shows the output of a selected job. This output is information on the progress of the program through the commands in real time. GRASP displays which command it is currently working on, the results of any convergence tests if performed, and an estimate of how much time remains in the current task, or a total elapsed time if it has already been completed. Figure 2-3 shows a Jobs window, with job output included on the right.

The final window shows a list of all completed jobs on the left, which can be

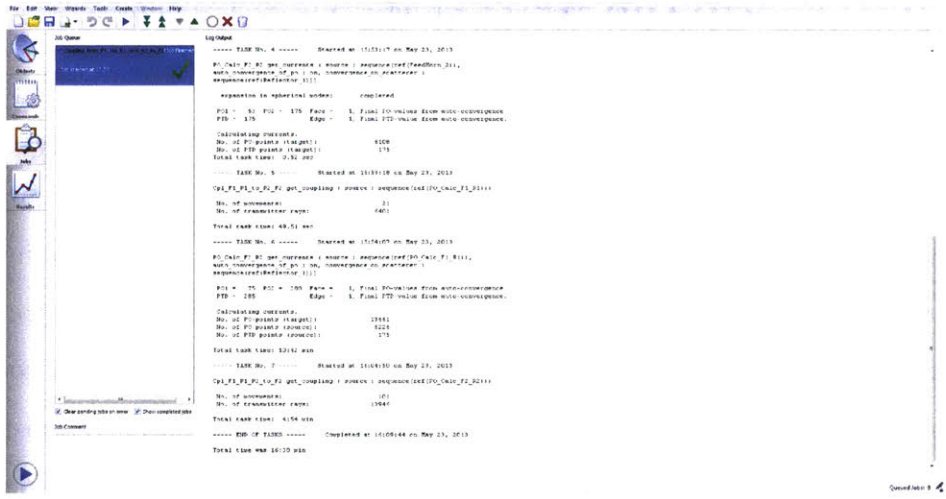

Figure 2-3: The layout of the GRASP Jobs window, with job output shown in the right panel from the scenario shown in Figures 2-1 and 2-2.

expanded to show which kinds of analyses were done in each. Clicking on these displays a plot of the output of that part of the job. Certain commands, such as "Get Field" or "Get Coupling," have a set of results for each instance of the command in a given job. An example window is shown in Figure 2-4, with the results of a simple coupling exercise on display on the right.

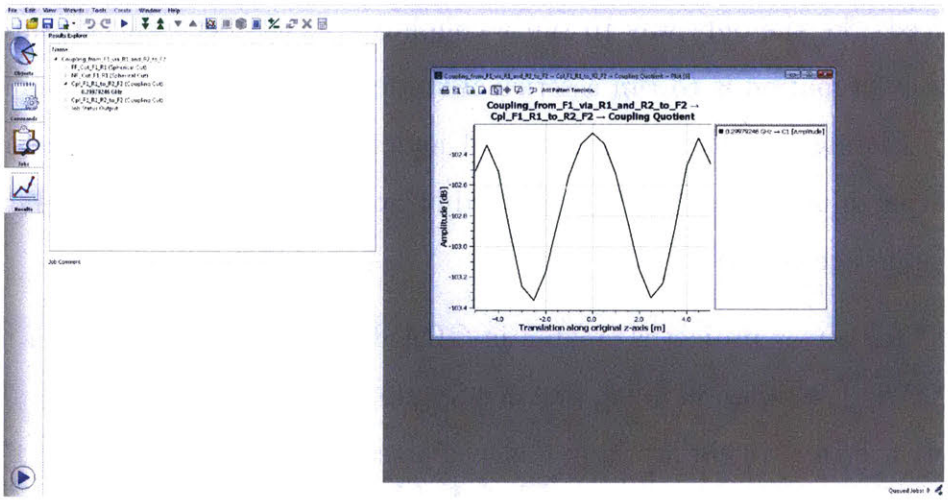

Figure 2-4: The layout of the GRASP Results window. Outputs are listed on the right, and clicking on them displays a plot of the results of that particular command, as shown here with an example coupling plot.

2.2.2 Running GRASP Without the User Interface

The GRASP user interface is straightforward and easy to use. Many projects are run successfully using it. However, it does introduce certain limitations, namely that it treats all objects as static in order to perform calculations. The coupling add-on does attempt to remedy this by introducing a "movement definition" object, which allows the user to move the receiver in a coupling scenario by selecting a coordinate system which hosts the receiver and specifying another coordinate system in which to move it. The direction or rotation, distance, and number of evaluation points can all be input into this movement definition. However, the key limitation of this object class is that it only moves the receiver, even if the coordinate system selected to be moved includes other objects. Even a reflectors are not moved, only their feeds. This is done so that currents can be calculated on all objects, and the only variable in that situation is the location and orientation of the receiver. Thus, if some scatterers are in a different position, currents and fields would need to be reevaluated as the currents induced on some of the objects on the others would no longer be constant. This is disadvantageous in a scenario where the receiver is fixed to a satellite, as some radiation scatters off of the satellite bus, and in many cases there is a reflector that goes along with a feed that greatly impacts the amount of energy that is coupled into the feed. So, the only way to run a coupling scenario between two satellites in which one is in motion is to run a series of static scenarios at different points along the path. Hitting the "Go" button several hundred times in rapid succession after each iteration is not a very efficient method of executing one of these scenarios, so a different approach is needed.

Every time a new project is created in GRASP, a folder is created with the main file (a GXP file), a separate folder entitled "working," and additional folders for each job as they are run. In the working folder is a second version of the main file called batch.gxp, intended to enable users to run GRASP in batch mode from the command prompt. Also included in the working folder are two additional files which are required for GRASP to operate: a TOR file which lists all of the objects created in the Objects

window, and a TCI file which lists all commands to be run. Both files are produced every time a user saves his or her progress in the main application. To run GRASP in batch mode, a user need only navigate to the working folder for the desired project, and run the grasp-analysis command, which uses the GXP, TCI, and TOR files to run the job just as if it was being done using the application. The output is printed to a file which then appears in the working folder.

The advantage of running GRASP in batch mode is that it allows runs to be scripted. GRASP can be called from a separate application, run, and the output can be read and processed all at once. For the satellite servicing scenario, what this means is that one script could be written in MATLAB that could call the grasp-analysis command multiple times. To do this, a separate MATLAB script is written to edit the TOR file. This function is capable of editing many different attributes of various objects, but its main and most important use is to change the origin of a satellite's coordinate system relative to the project's overall coordinate system, resulting in the two satellites moving relative to each other. To perform coupling scenarios, scripts are written that create vectors of coordinates for one satellite to move along and then loop through each of these coordinates, editing the TOR files in each iteration before invoking the command prompt to run the grasp-analysis command. After each iteration, a separate function is used to read the output file and store the cumulative results in a workspace variable. At the end of the script, these variables are saved to a MAT file which could be read later.

A complicating factor in writing these scripts is that as the satellites move, their relative orientations change, meaning that the surfaces that the radiation is scattering off of change throughout the scenario. The solution to this is that each scenario needs its own separate script to account for differences between them, and sometimes multiple TCI files are needed, along with code included in the main script that would convert each of them into the main TCI file that GRASP expects (the one with the same name as the project and GXP files) when needed.

Chapter 3

Approach

The content of this chapter deals with how GRASP is utilized to determine the level of coupling between the servicing satellites and their clients. It begins with a comparison of the GRASP output to expected far-field results of the Friis equation. It then discusses the models of both servicers and a generic client made within GRASP for the analysis. After this, it describes the ways these models are used to simulate realistic use cases and determine the levels of RF coupling that would exist in these situations. Finally, it also details some of the computational issues that arose in practice and how they are mitigated.

3.1 Validation

To validate the approach of running many iterations of individual coupling calculations sequentially and to ensure the GRASP output is along the lines of what is expected, a simple scenario is devised to ensure everything is working properly. This scenario, shown in Figure 3-1, includes two 1 m reflector antennas operating at 12 GHz (the GRASP default frequency), fed by free floating feeds directly in front of them. These reflectors are aligned so that they face each other, with their boresights lined up on the same axis.

Once this scenario is set up, a script is written to keep one of the reflector-feed pairs stationary while the other moves outward from a distance of 2 m to 200 m,

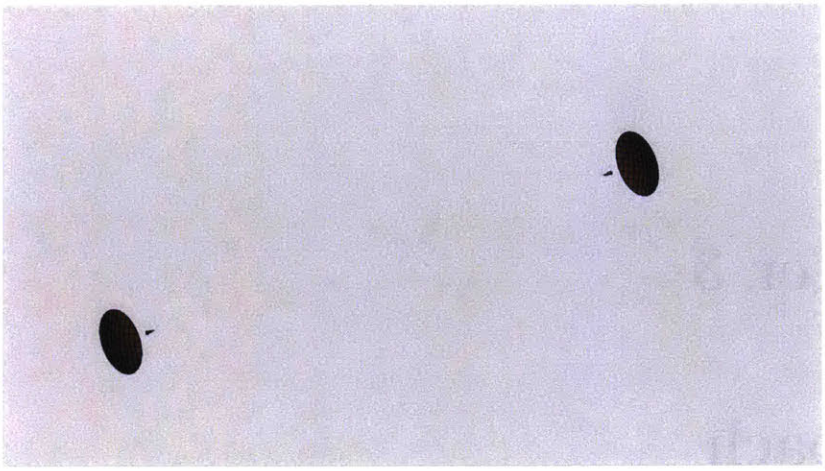

Figure 3-1: A simple scenario with two 1 m reflectors pointing directly at each other, shown here at a distance of 10 m.

calculating the coupling from the first feed into the second feed at every step. The final plot of the coupling serves multiple purposes. First, it verifies that the decibel (dB) units output by GRASP are in fact dBW, with respect to 1 Watt. Second, it shows that the method of editing the TOR file to move multiple objects at once and doing this over a large number of iterations is a reasonable way to show a variation in the coupling coefficient over a large distance. And finally, when compared with the predicted coupling numbers from Equation (2.7) it provides a clear illustration of the effects that the near-field has on coupling versus using a far-field model when two antennas are close to each other. The comparison also shows somewhat indirectly how GRASP deals with antenna aperture efficiency. In Figure 3-2, the plot on the left shows the direct comparison between the GRASP output and what the Friis equation says the coupling should be. At small distances, the GRASP coupling levels off, while the Friis coupling continues to rise asymptotically. This can be attributed to the antennas being in the near-field of each other, in a region in which the Friis equation is ill-suited to describe. At larger distances, the slope of the two plots seems to converge, with the Friis coupling seeming to reach a consistent level of 3 dB higher than the GRASP coupling. This seems to suggest that GRASP uses an aperture efficiency value of $\frac{1}{\sqrt{2}}$ when doing its calculations. Applying this value to Equation (2.6) to plug into Equation (2.7) gives a Friis coupling that is much closer to the

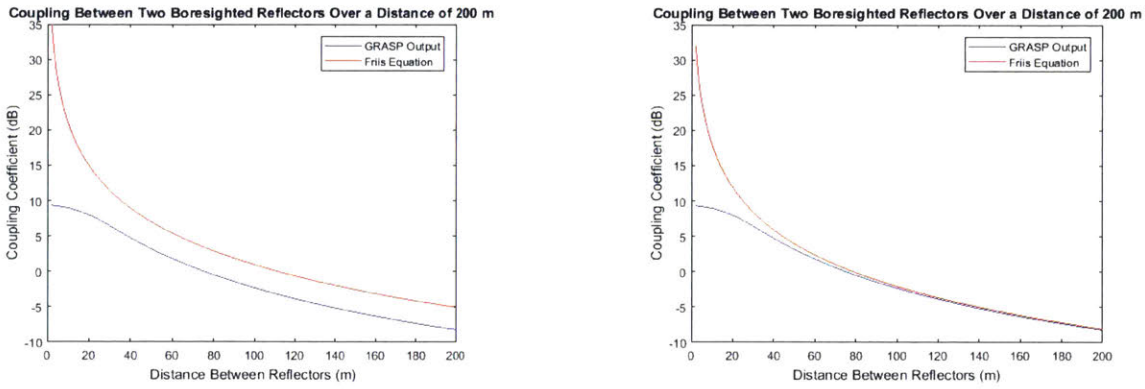

(a) (b)

Figure 3-2: (a) Comparison of boresighted reflector scenario with Equation (2.7), with the value of ε_a from Equation (2.6) set to 1. (b) The same comparison, with the value of ε_a set to $\frac{1}{\sqrt{2}}$

GRASP coupling, and is shown on the right in Figure 3-2.

3.2 Satellite Models

Once the program output was understood, models needed to be made of each satellite to understand the interactions that occurred between them. Detailed Computer Aided Design (CAD) models of the satellites in question (MEV-1, RSGS, and Intelsat 901) are not available and are considered to be proprietary information to their respective manufacturers and operators, so many details of the GRASP models are interpreted from publicly available documents. In the cases of the MEV and RSGS, as these satellites are not yet complete, this information is heavily based on the artists' renditions of the spacecraft. It should be noted that the actual designs of these spacecraft may ultimately differ greatly from the publicly available artwork, but it is also the case that this thesis is more concerned with RF coupling on any possible future servicing mission and not necessarily these two in particular. The advantages of performing case studies with the MEV and RSGS programs is that they present two different communications architectures. The differences can be analyzed to get a clearer view of how the inter-spacecraft coupling works and how it can be mitigated. Thus the important part of modeling these satellites is accurately representing the

communications architecture; the remaining parts of the satellites can be low fidelity representations to make the results more broadly applicable to a wide range of situations. The following sections detail the considerations that went into making the models of each satellite.

3.2.1 Client

The model of the client is the one with the most ambiguous specifications; Intelsat 901 has been named as the first client of MEV-1, but this will likely not be the only client serviced by MEV-1, and RSGS may well have a large number of clients, none of which have yet been named. This necessitates a model of a "generic" client, one that still has features one would expect a geostationary satellite to have, but that does not have any distinguishing features that make the results too specific to that one case. A look at the business case for a servicing satellite finds that most of its customers would be in fields such as communications or government, with the communications sector having a strong financial incentive to extend the lives of its satellites if feasible. For this reason, the client is modeled after a communications satellite. Specifically, it draws inspiration from a CAD model of Intelsat 7 used as a satellite representation in Systems Tool Kit (STK), a systems modeling and simulation software. Figure 3-3 shows images of this model from STK. [5]

The main features drawn from this model are the two reflectors on either side of the bus and the set of smaller reflectors on the nadir-facing panel of the bus fed by four feeds on struts attached to the bottom of the satellite. These features are emulated to create the client model shown in Figure 3-4.

The model includes six plates that make up a 2 m by 2 m by 3 m bus. The bus is assumed to be conducting; additional features that would be on a real satellite such as MLI are excluded from the model. On either side of the bus are 1.5 m diameter parabolic reflectors attached to the top of the bus by two struts each and fed by feeds attached to the side panels. On the other two side panels are the solar arrays, modeled as 8 m by 2 m. The solar arrays are placed in their own separate coordinate system based in the client coordinate system so that they could be rotated together

Figure 3-3: Two views of a model of Intelsat 7 from STK. [5]

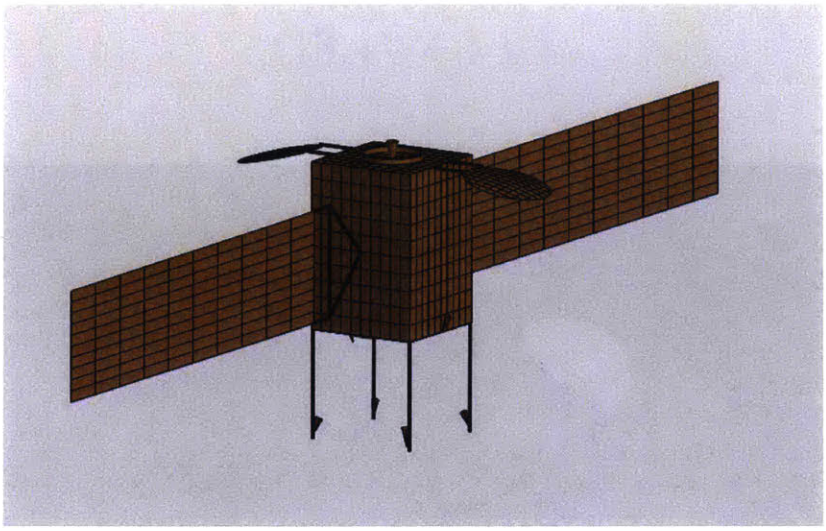

Figure 3-4: The model of a generic client satellite to be used in coupling calculations. The bus has a 2 m by 2 m base and is 3 m tall, with 8 m by 2 m solar arrays.

cohesively, but this feature is not used much during the analysis. On the top panel of the bus are features representing the launch adapter ring and LAE, which are used by the servicing spacecraft for docking and grappling the client. Figure 3-5 shows a view of the bottom of the spacecraft, which houses four smaller reflectors reminiscent of the Intelsat 7 model, as well as the feeds for all four of the reflectors on struts attached to the bottom bus panel. Three of these reflectors are 0.8 m in diameter, while the fourth is 0.7 m. The reasons for this are discussed in Section 3.4.

Each of the six feeds on the client can be set to operate at different frequencies. To align with the proposed frequency bands of the MEV and RSGS, both C-band and Ku-band are used for parts of the analysis. As GRASP only operates in discrete frequencies, four frequency bands are defined for use in this project, spanning the FCC defined GEO communications satellite frequency bands and including six equally spaced discrete frequencies in each. These are the C-band transmit from 3.7 GHz to 4.2 GHz, the C-band receive from 5.925 GHz to 6.425 GHz, the Ku-band transmit from 11.45 GHz to 12.25 GHz, and the Ku-band receive from 13.75 GHz to 14.5 GHz. The lower frequencies lead to larger display sizes for feeds in the model, leading to the discrepancy that may be noticed between the two side feeds in Figures 3-4 and 3-5. In addition to this, each physical object must have a corresponding electrical object

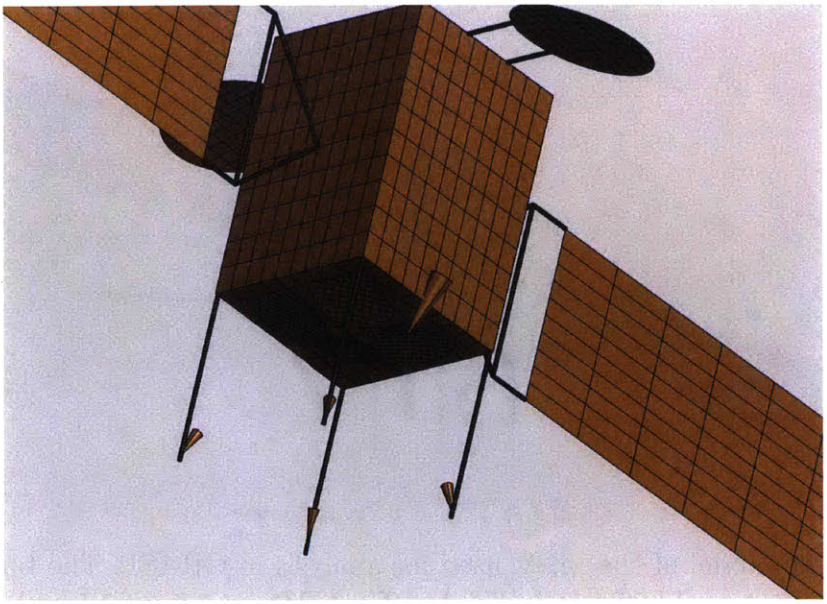

Figure 3-5: The GRASP Client model viewed from below.

specifying a frequency or a frequency range if an analysis is to be done on it. These objects are toggled between C-band and Ku-band as the situation warrants. To make for a more realistic model, the solar arrays are coated with a dielectric layer with a dielectric constant similar to that of glass to simulate actual solar arrays which would not be covered in a conducting material. Due to this, GRASP is not able to perform a PTD analysis on the solar arrays, though it is able to use PO. All other objects are assumed to be made of conducting material.

3.2.2 MEV-1

The MEV program has the advantage of being far enough along that it has documentation filed with regulators that is available for public viewing. This documentation, particularly from the FCC, is instrumental in understanding the MEV's proposed communications architecture. However, structural designs for the satellite are still proprietary information, and so the majority of the satellite model remains to be derived from artists' renditions and animations of the satellite's mission and CONOPS. Figure 1-1 shows one such rendition, and the features it shows are replicated in the GRASP model, shown in Figure 3-6.

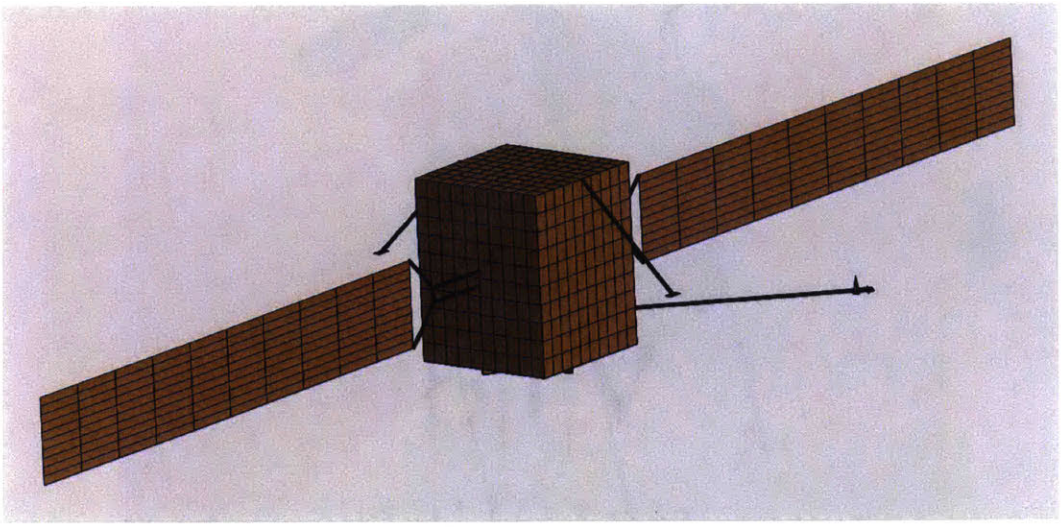

Figure 3-6: The model of the MEV used for analysis in GRASP. The bus consists of a 2 m by 2 m base, and is 2.5 m in height. The solar arrays are 1.5 m by 10 m.

The MEV model is relatively simple. It consists of six plates, forming a 2 m by 2 m by 2.5 m bus. It has two solar arrays attached by structures similar to those seen in Figure 1-1. These solar arrays are treated similarly to the client solar arrays in that they are given a separate coordinate system and coated in a dielectric layer to simulate glass. The model emulates the planned electric propulsion modules by using a long strut with a plate on the end on either side of the bus, however this is simply an aesthetic feature with little to no functionality, as is discussed in Section 3.4. It also includes a very simplistic representation of the MEV's docking stanchions, shown more clearly in Figure 3-7.

Figure 3-8 shows two views of the orientation of the MEV and client when docked. This also gives some insight into the relative positions of the transmitters and receivers on each satellite during servicing operations.

The final feature on the MEV model is the TCR boom. In the GRASP model, this is represented as another strut with a small plate on the end, but this time the plate hosts four antennas, one in each frequency band (C-band and Ku-band transmit and receive). FCC filings show these antennas to be HEMI, or hemispherical antennas, with a radiation pattern consisting of one large lobe in front an a smaller one in back. The filings also show a nominal power input into the antennas as well as gain values at

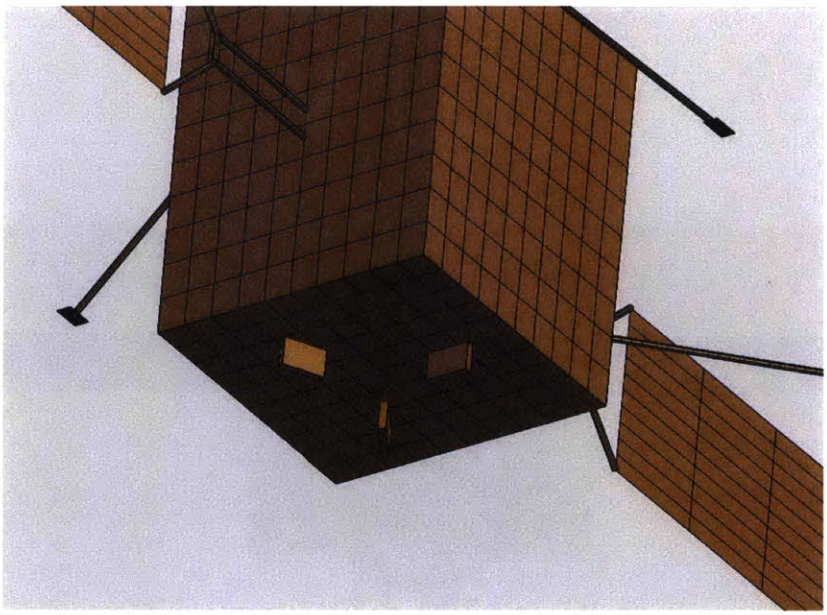

Figure 3-7: A view of the underside of the MEV model, showing a low fidelity representation of the docking mechanism.

several select angles from the antenna boresight. Specifically, these figures are 20 W input power for the Ku-band antenna, 30 W input power for the C-band antennas, a gain of 5 dB at an angle of 17°from the antenna boresight on all antennas, and a gain of -7 dB at an angle of 75°from boresight. In GRASP, a hemispherical antenna is best represented by an object of the "cardioid pattern" class. Using this object, parameters are varied in order to form a radiation pattern that meets the gain specifications at all four points mentioned in the FCC filings. The final parameters are a co-polarization beamwidth of 75°, a cross-polarization beamwidth of 45°, and a front to back ratio of 20. This produces the pattern shown in Figure 3-9b. From there, the transmit power can be added in as an amplitude factor in the antenna object or as a simple offset in coupling data once already produced.

3.2.3 RSGS

The model of the RSGS program's RSV is left mostly to speculation, as whatever plans existed for the bus are rendered obsolete with the withdrawal of SSL from the RSGS contract. Thus, the basis of the GRASP model is ultimately artists' renditions

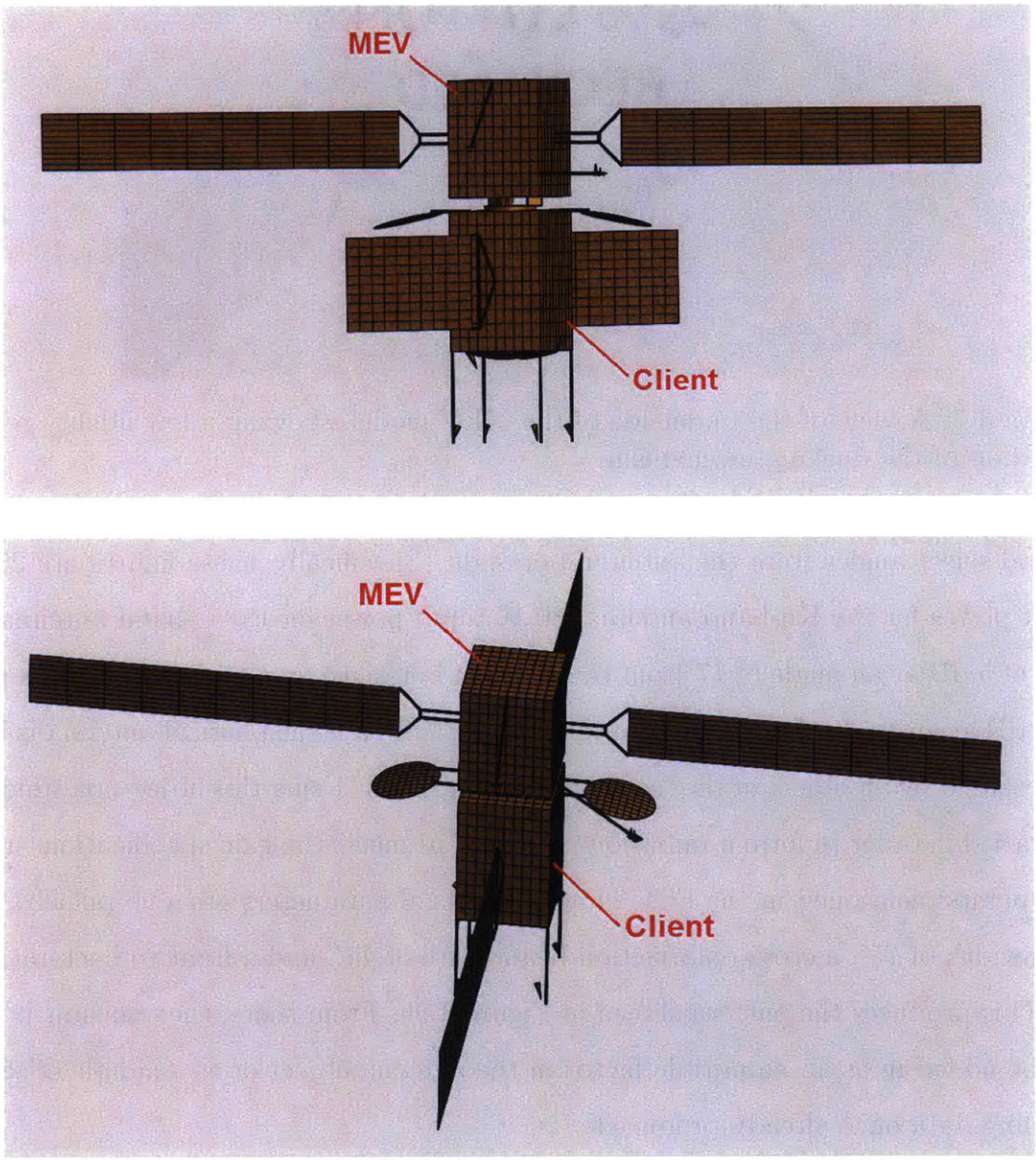

Figure 3-8: Two views of the MEV docked to client for servicing operations.

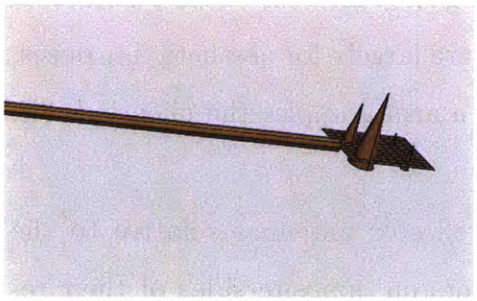

(a)

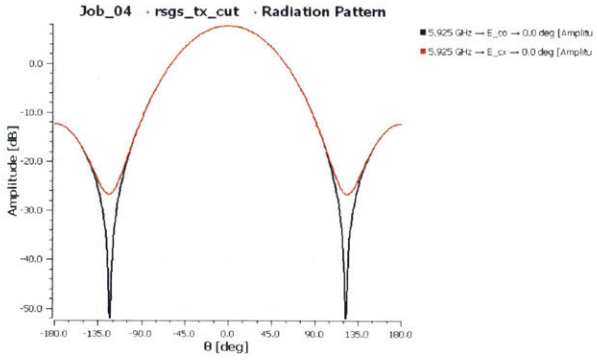

(b)

Figure 3-9: (a) A simplistic representation of the MEV TCR boom. Four HEMI antennas are shown installed on the end of the boom. (b) Simulated antenna pattern for one of the HEMI antennas before accounting for transmit power.

commissioned by DARPA from before the contract was even awarded, such as that in Figure 1-3. Among the major features shown by these illustrations are the robotic arm payload, the main bus, a single solar array on one side of the bus, and a pair of parabolic reflectors on opposite sides of the bus. These features are translated into GRASP as shown in Figure 3-10.

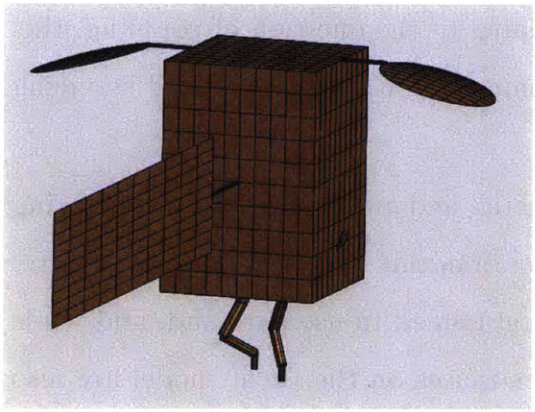

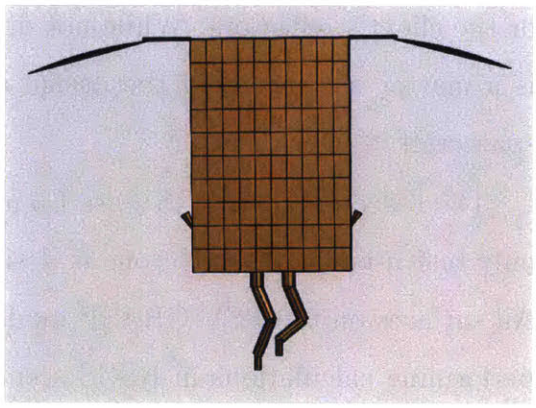

Figure 3-10: Two views of the RSGS GRASP model. The RSV model shares its dimensions with the client model, with a 2 m by 2 m base and 3 m height. The solar array is also 2 m by 8 m, although the RSV only has one.

In GRASP, the bus is again represented by six plates forming a 2 m by 2 m by 3 m rectangular prism. The solar array, only on one side of the bus, is attached by a single strut this time and is again coated in a dielectric layer. The robotic arms are formed

by 8 struts whose relative orientations can be changed to simulate manipulation of the arms, but this feature and the arms themselves are largely for aesthetic purposes, and mainly used to simulate the scenario in which a arm grapples the client's LAE. Such a scenario is shown in Figure 3-11.

Also of note is the orientation of the RSV's reflector antennas relative to the client's. Both the RSV and the client have reflectors on opposite sides of their respective buses, so the RSV is grappled to the client such that its reflectors are angled 90°relative to the client's to prevent shadowing of its signal and to ensure reception on the Earth. This configuration also shows that the RSV as it is represented here is very susceptible to having some part of the client physically block parts of its transmit or receive beam, interrupting communications between the satellite and its Mission Operations Center (MOC). Such a scenario can be envisioned if one imagines that the gap between the solar arrays and the client bus were slightly smaller, with the arrays tracking the sun and temporarily positioned horizontally rather than vertically. In this case, if the RSV wished to communicate, it would have very few angles at which to position itself on the client so that is is not shadowed by either the solar arrays or the client's reflectors. While not directly related to the question of coupling, this is a matter of concern in the design of a communication architecture for servicing spacecraft.

The reflectors on the RSV are 1.5 m in diameter, and are assumed to be operating only in Ku-band. As such, one is designated for transmit and the other for receive. All surfaces on the RSV GRASP model are programmed to use Ku-band, and while performing calculations in RSGS scenarios, all surfaces on the client model are also set to Ku-band.

3.3 Scenarios

With the GRASP models created, this section describes how they are used to determine the levels of RF coupling that might be seen on orbit. While by no means exhaustive, these scenarios incorporated known details from the CONOPS of both

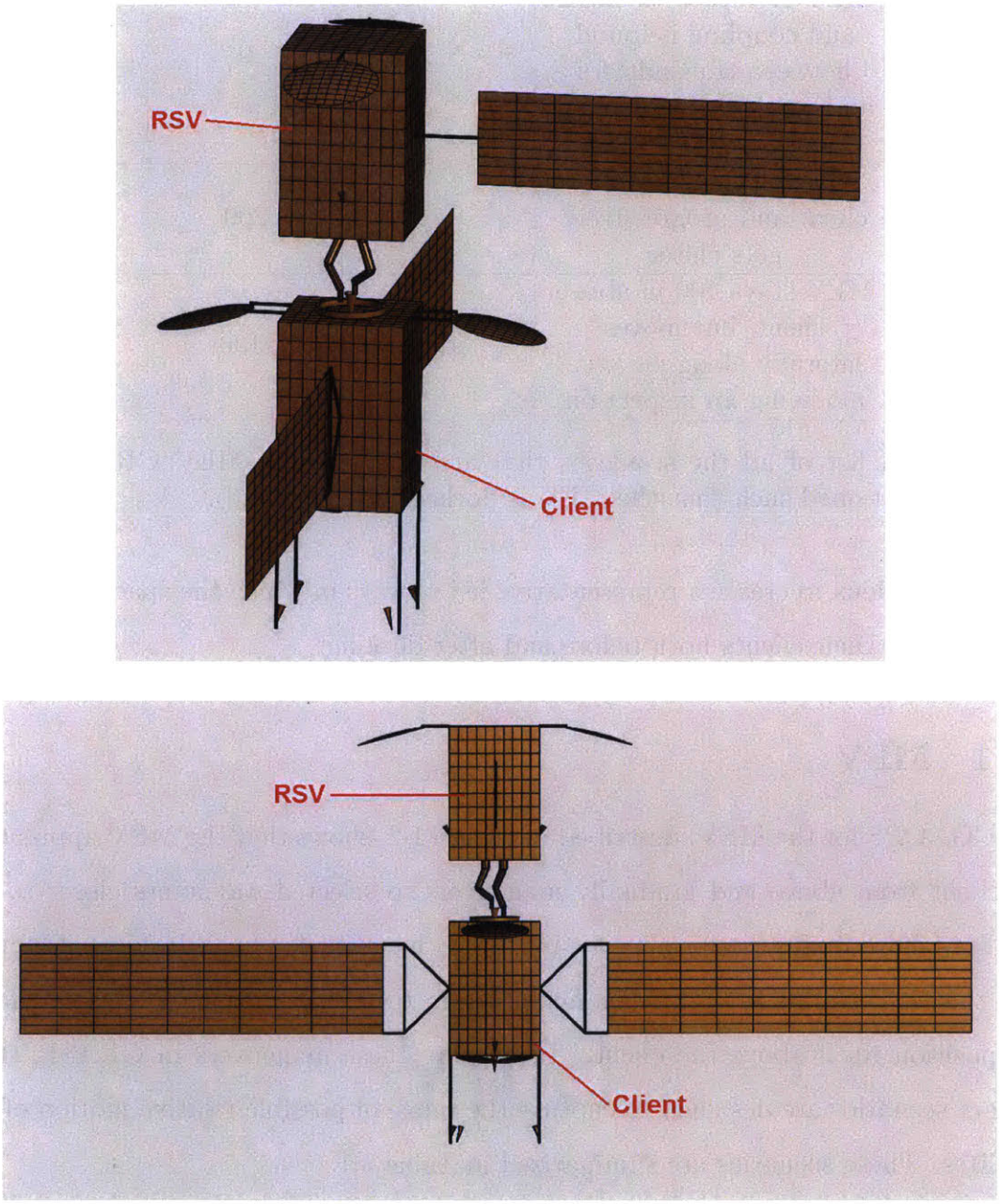

Figure 3-11: Two views of the RSV grappled onto the client's LAE for servicing operations. One arm can be seen grabbing the structure while the other is free to move around and service other parts of the client.

Name	Description	Movement Axis	Starting Point (m)	Ending Point (m)
Docked	Operational case, where MEV is docked to client and coupling is found between transmitters and receivers at planned operational levels	N/A	0	0
Approach	MEV starts 200 m above client and progressively gets closer	z	200	0
Flyover	MEV stays 100 m above client, but moves laterally along an axis, modeling an inspection	x, y	-100	100

Table 3.1: A list of all the scenarios that are run with the MEV GRASP model. Client is positioned such that the MEV is docked to it at (0,0,0).

planned missions to create a representative list of ways in which the spacecraft might interact with their clients both before and after docking.

3.3.1 MEV

The CONOPS for the MEV, described in Figure 1-2, shows that the MEV approaches the client from above and gradually maneuvers to selected waypoints closer to the satellite before finally performing a capture of the client for final docking. Before it does this, it performs a rendezvous maneuver in the GEO graveyard orbit so that it can position itself above the client. To capture these maneuvers in GRASP, three distinct scenarios are designed to capture the range of possible relative motion of the satellites. These scenarios are summarized in Table 3.1.

The first scenario is the fully docked case, where the MEV is attached to the top of the client and actively controlling the attitude and propulsion of both spacecraft. The next scenario is drawn directly from the CONOPS. It involves the MEV starting at a point 200 m directly above the client and moving closer, at a step of 0.5 m, until it finally docks with the client. This serves to demonstrate the coupling during the RPO phase immediately before docking. The final scenario is essentially two different

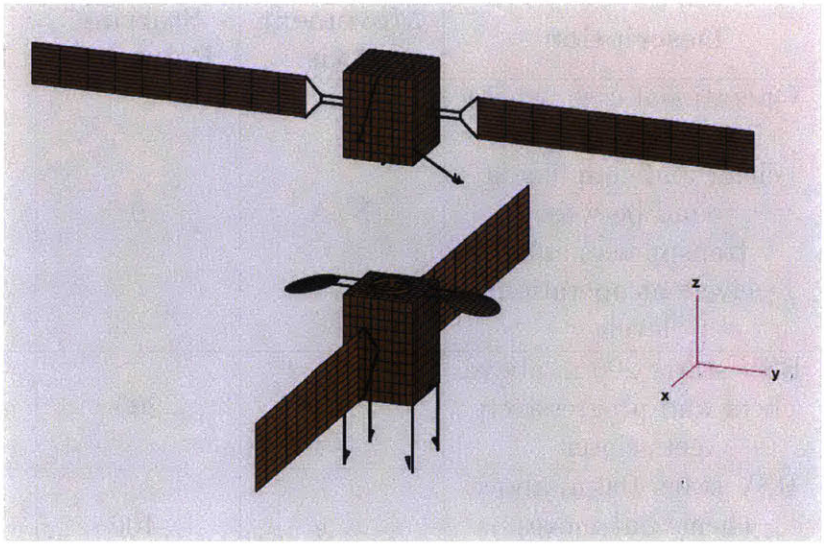

Figure 3-12: A view of the MEV above the client at close quarters with a set of Cartesian axes added to demonstrate how the MEV moves relative to the client in the coupling scenarios.

scenarios, and it involves the MEV performing a "flyover" of the client at a distance of 100 m. In both of these, the distance from the servicer to the client in the z direction remains constant, but the servicer moves from -100 m to +100 m with a step of 0.5 m, first in the x direction and then in the y direction (these are done separately, while varying x; y is held constant at 0 m, and vice-versa). Figure 3-12 shows a diagram of the client and MEV separated by approximately 5 m, with coordinate axes added for clarity in understanding the scenarios.

3.3.2 RSGS

The RSGS CONOPS, while not yet as detailed, is more expansive than its MEV counterpart. It shows the RSV performing the same type of rendezvous maneuver in the GEO graveyard to get within range of the client. Then it goes into a proximity operations period, in which the RSV is shown circling around the client taking imagery and building up a model of the client before approaching it. Once it is done with this, theRSV approaches its client. It is not specified, but it is assumed that theRSV will also approach from above, as it will be grappling onto the LAE and will be attempting to avoid interfering with the client's operations during the RPO phase. These aspects

Name	Description	Movement Axis	Starting Point (m)	Ending Point (m)
Docked	Operational case, where RSV is grappled to client and coupling is found between transmitters and receivers at operational levels	N/A	0	0
Approach	RSV starts 200 m above client and progressively gets closer	z	200	0
Flyover	RSV stays 100 m above client, but moves laterally along an axis	x, y	-100	100
Inspection	RSV circles the client at a distance of 100 m, simulating inspection and taking imagery	θ_{yz}, θ_{xz}	0°	360°

Table 3.2: A list of all the scenarios that are run with the RSGS GRASP model. Client is positioned such that RSV is grappled to its LAE at (0,0,0).

of the CONOPS are translated into the scenarios in Table 3.2, which are essentially the same scenarios as the MEV with the addition of an "inspection" scenario.

The first three scenarios (Docked, Approach, and Flyover) are direct duplicates of the MEV scenarios. In addition to covering some aspects of the RSGS CONOPS, this allows for a direct comparison between the two types of communication architectures used and how the coupling levels differ between the two. The Inspection scenario, however, is unique to RSGS. In it, the RSV goes in a circle around the client at a constant distance of 100 m with a step size of one degree. Separate scenarios are run for rotation around the x-axis and the y-axis. In these scenarios, the RSV is always pointed nadir, as if it is communicating with the ground, rather than pointed at the client as if it is actively taking imagery. This is to simulate the act of the RSV transmitting its imagery to its MOC during the inspection phase rather than the act of inspection itself, as the RSV will presumably not be transmitting while it is pointed at the client to take images. Figure 3-13 shows the orientations of the RSV

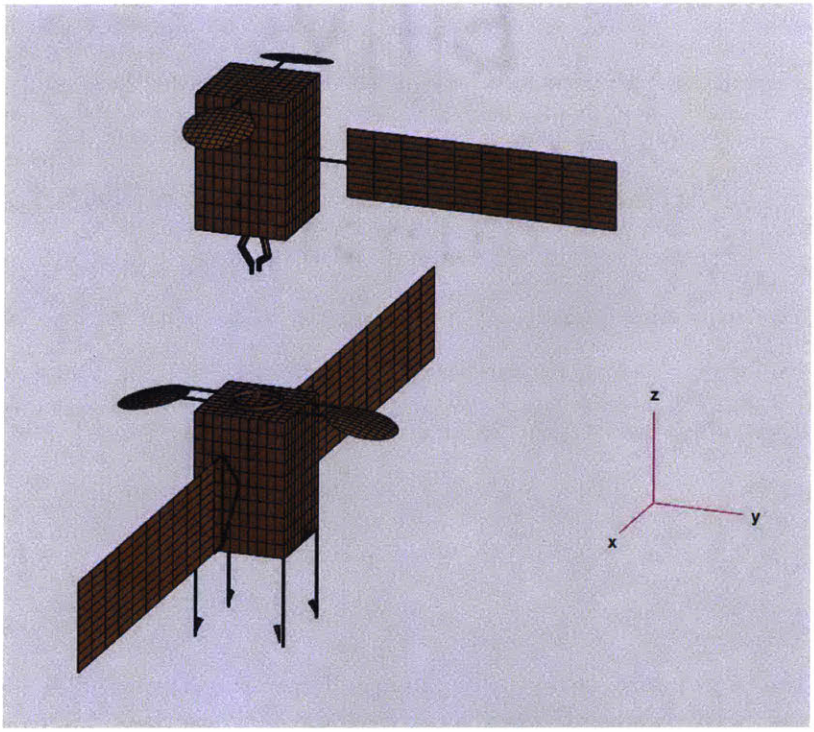

Figure 3-13: A view of the RSV above the client at close quarters with a set of Cartesian axes added to demonstrate how the RSV moves relative to the client in the coupling scenarios.

and the client at a distance of approximately 5 m in the z direction, along with a set of coordinate axes to make clear the movements outlined in Table 3.2.

3.4 Computational Considerations

One of the greatest challenges in undertaking this project was that of computational efficiency. While calculating a field pattern in GRASP could be done in a matter of seconds or minutes, calculating coupling can potentially take far longer. This is because of the way coupling is calculated. In calculating currents on objects, GRASP includes a setting called "ray output" which when set to "all" calculates a ray from every current element which can then be used in subsequent current, field, and coupling calculations. This is much more time consuming as it calculates the direction of each field element individually rather than assuming the field is moving in the direction of the overall Poynting vector. However, if coupling is to be computed,

ray output must be set to all, as this is the only way to consider the magnitude of each current element in the direction of the receiver. This leads to much longer run times not just for the coupling calculation, but for all the current calculations leading up to it. The problem is amplified when considering radiation reflected off of multiple scatterers. Each current element on a given scatterer must contribute a ray to each current element on a subsequent scatterer, leading to an approximately exponential slowdown in run time if a job is structured in this way. This is what is meant by a "high fidelity" coupling calculation, as it is the most accurate and takes into account a great number of features of the model. However, a calculation of this sort may take many days or even weeks to complete, making it infeasible if one wishes to run many of them.

Several steps are taken to cut down enough on run times such that scenarios of several hundred iterations can be performed. The first is to exclude all minor scatterers, such as struts and other fixtures that do not contribute much to the overall calculation and slow down run times greatly, from the calculations. This leaves plates and reflectors as the major sources of scattering in most scenarios. The next step is to limit the paths of the radiation off of scatterers such that each path included no more than one without losing fidelity in the overall calculation. With the MEV, this is more or less straightforward. Currents are found on each of the reflectors and plates that are determined to be illuminated by the transmitting antenna, and coupling is found between the selected receiver with each of those scatterers and the original transmit antenna as sources. With RSGS it is a little more difficult, as the main antenna pattern interacting with the client is produced by a reflector, meaning that any radiation scattered off of a surface on the client is already being scattered off of two surfaces in series. The way around this is to split the coupling calculation into two parts, one finds the coupling only from the RSV's reflector and its feed while the other finds the currents on the RSV's reflector with "ray output" set to none, and then uses this as a source to calculate the currents on the remaining scatterers with "ray output" set to all. With these changes implemented, iterations of scenarios range from approximately two minutes on the low end, to ten minutes and sometimes

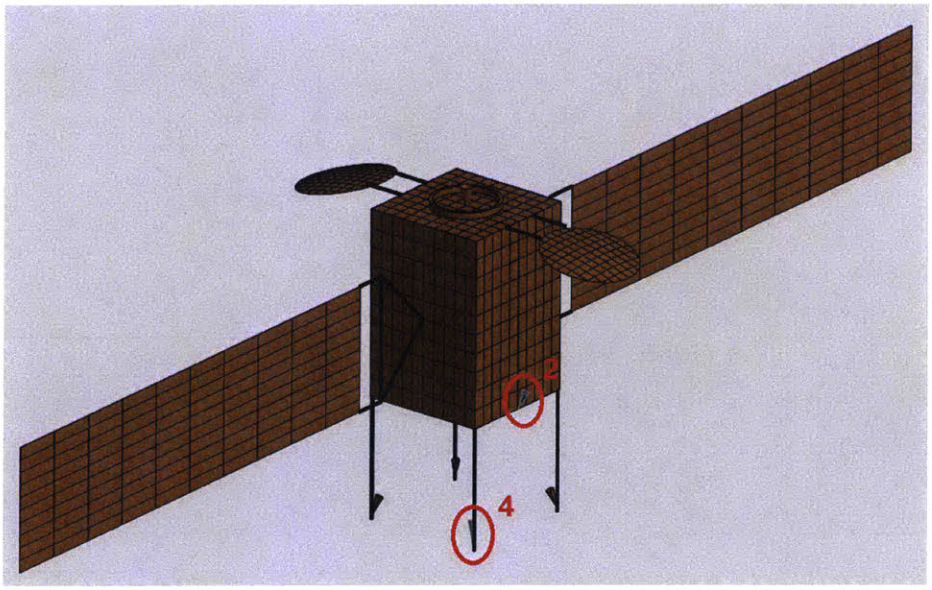

Figure 3-14: The model of the client satellites with the feeds used for analysis highlighted in green and circled and labeled in red.

higher on the high end. However, this is still enough of an improvement to make full runs of the scenarios in Tables 3.1 and 3.2 possible.

The time taken to perform the computations depends greatly on the computer used, and more specifically on the number of CPU threads available on a given machine. This is due to the parallelizable nature of the calculations, as calculating currents from one element is independent of calculating the current from another element on the same object. Most of the scenarios were run on MIT Lincoln Laboratory's CAD grid, which has nodes with 24 Central Processing Unit (CPU) threads each. Additional scenarios were run on a desktop computer at Lincoln Laboratory; this machine only has 12 CPU threads available and therefore took approximately twice as long to run. The total run times for each scenario are shown in Table 3.3.

Another computational issue arose during some of the scenarios that was initially a bit puzzling. In the "approach" scenarios there was a disruption in the data that sometimes manifested as a large spike in the magnitude of the coupling coefficient and other times as a discontinuity in an otherwise smooth plot. These anomalies were seen across frequencies and receiving antennas, and consistently occurred in the vicinity of $z = 50$ m. While the exact cause is unknown, it was determined that they were due

Scenario Type	Servicer	Band	Feed	Iterations	Threads	Time (h)
Approach	MEV	C	2	401	12	12.92
		Ku	2		24	18.28
		C	4		12	12.94
		Ku	4		24	18.34
y-axis Flyover		C	2		12	17.84
		Ku	2		24	21.59
		C	4		12	17.92
		Ku	4		24	21.70
x-axis Flyover		C	2		12	17.62
		Ku	2		24	22.26
		C	4		12	17.68
		Ku	4		24	22.26
Approach	RSGS	Ku	2		24	46.40
			4		24	46.66
y-axis Flyover			2		24	49.64
			4		12	74.43
x-axis Flyover			2		24	47.90
			4		12	70.27
yz Inspection			2	360	24	93.98
			4		12	184.38
xz Inspection			2		24	74.48
			4		24	86.10

Table 3.3: A table showing the amount of time each scenario took to run, along with several relevant computational parameters. In the table, feed "2" refers to one on the side panel of the client, while feed "4" refers to one attached to a strut on the underside. These are highlighted in Figure 3-14.

to the placement of the receivers relative to the scatterers. The display size of a feed or cardioid pattern object in GRASP is related to its frequency; if the frequency is increased, the object gets smaller, while if it is increased, the object becomes larger. In some cases, this led to the feeds on the sides of the client bus intersecting the plates on which they are supposed to be mounted. When the combined feed-reflector coordinate system is shifted slightly so that the feed is then free floating, the anomaly then disappears. While it seems intuitive that part of the feed being inside the bus was the cause of the problem, this was not the case for the feeds on the bottom of the client. These feeds were not even directly underneath the edges of any of the side plates, and the only objects they were intersecting were struts which were excluded from the calculations to save computation time. Yet they still exhibited this anomalous behavior, and in some cases it was even more severe than with the feeds that were intersecting plates. Ultimately, the feed used for calculations had to have its x and y coordinates adjusted to 0.75 from 0.9 in order to fully remove the spikes from the data. The reflector associated with this feed was also reduced in diameter from 0.8 m to 0.7 m. As the client satellite is considered more or less symmetric, coupling is calculated into a single feed on the side of the satellite and a single feed on the bottom, with these two being seen as representative of all other feeds situated similarly. Each of the feeds on the client is assigned a numerical designator; the ones used for the calculations are labeled "feed 2" for the side feed and "feed 4" for the bottom one. Figure 3-14 shows the location of each feed on the client and labels them for clarity. The effects of the modifications to these two feeds can be seen in some of the images of the client model in previous sections, particularly in Figures 3-8 and 3-11. The contrast is especially stark between feed 4 and the other three on the bottom of the client that are not used for calculations, as it can be seen floating at a distance from the strut it is supposedly attached to while the others have retained their positions on their struts. The situation is the same but less obvious for the side feeds. Ultimately, the shift of these two feeds allowed the scenarios to continue forward without any more anomalies in the data. Figure 3-15 shows portions of a scenario run before and after the change was made.

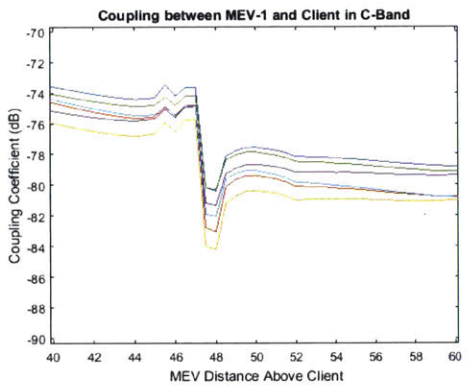

(a)

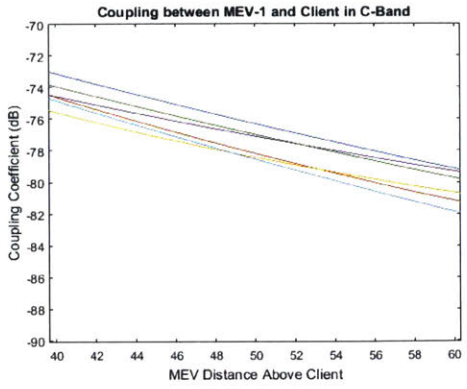

(b)

Figure 3-15: (a) The region of 40 m to 60 m in the "approach" scenario for the MEV, showing a discontinuity in the data before the receive feed (feed 2) was moved. Each curve represents a frequency in the range of 3.7 GHz to 4.2 GHz, in increments of 100 MHz. (b) The same region and the same scenario with feed 2 shifted over slightly. The data for all frequencies has been rendered smooth and continuous.

3.5 A Note on Polarization

Looking back at Equation (2.29), a large contribution to the overall coupling coefficient is the $\mathbf{E}_t(r, \theta_t, \phi_t) \cdot \mathbf{E}_r(r, \theta_r, \phi_r)$ term. The direction of each electric field vector is the field's polarization, and depending on the angle the transmitting field makes with the receiving field, this dot product may end up being rather large or small. GRASP has four options for polarization: linear x, linear y, right hand circular, and left hand circular. Each of these polarizations is defined in the coordinate system of its respective feed, with the implication being that even if two feeds nominally are set to the same polarization, if they are at an angle to each other their polarization vectors will not line up. This project uses a number of sources at various angles, and rather than attempt to rig the polarization of the feeds used to produce the largest possible coupling values, a standard is set that all feeds would use a "linear x" polarization, with one exception. FCC documentation for the MEV shows that that spacecraft is being designed to use Right Hand Circularly Polarized (RHCP) and Left Hand Circularly Polarized (LHCP), and can switch between the two. [28] As such, the transmitters on the MEV GRASP model are set to "right hand circular." Keeping all the rest of the feeds at a standard polarization allows for a more direct comparison

between scenarios, and to more clearly see the effect that feed positioning has on the final coupling result.

In order to both get a clearer picture of how varying the polarization affects the amount of energy coupled into a receiver and to determine the potential worst case scenario which would result in the highest levels of coupling, each scenario would have to be run a total of sixteen times to reflect each combination of transmitter and receiver polarizations (for the MEV, this number would be eight, as the cardioid pattern object only allows circular polarizations). As this would greatly increase the amount of computation time for an overall small amount of additional information, this approach is not taken. Instead, each scenario is run once to produce a plot which showed how the coupling changed over the distance covered using the default polarizations, and then this data is used to identify points where there are peaks in the coupling coefficient. At these points, the scenario is run again, this time varying polarization rather than position. The outcome of the polarization variation is then used to determine both the worst case and best case coupling into the receiver. In many cases, the peak in coupling occurred at different points for different sample frequencies used. In these cases, there is often one frequency that had slightly higher coupling than the rest, and the polarization analysis is run using that frequency at its peak. The results of the polarization analysis are shown along with each scenario, primarily in Sections 4.1.2 and 4.2.2.

Chapter 4

Results

This chapter discusses the results of the scenarios outlined in Tables 3.1 and 3.2. Each scenario involving the MEV GRASP model is run a total of four times; two in C-band and two in Ku-band, with one of each of those calculating coupling into feed 2 and the others calculating coupling into feed 4, with the feeds numbered as shown in Figure 3-14. The scenarios involving the RSGS RSV model are run twice each; as only Ku-band is used in these cases, the scenarios are only run once for feed 2 and once for feed 4.

A full receiver sensitivity analysis is done in Section 5.2, however the results of this show that a typical received power from a ground station would be -84.1 dBW in C-band and-76.8 dBW in Ku-band. Coupling above these thresholds would overpower a signal sent to the client, essentially preventing it from communicating. The threshold for damage depends on the exact hardware used, but a typical value is around -30 dBm, or -60 dBW. It is to these values that the following data should be compared.

4.1 MEV Results

4.1.1 Docked

The first scenario examined what the coupling levels would look like with the MEV docked to the client. These levels, shown in Tables 4.1 and 4.2, are calculated in

Feed	3.7 GHz	3.8 GHz	3.9 GHz	4.0 GHz	4.1 GHz	4.2 GHz
2	-75.958	-76.648	-75.941	-76.774	-75.850	-77.703
4	-121.385	-129.963	-134.798	-132.479	-127.362	-122.153

Table 4.1: The coupling coefficients in dBW of the interactions between the MEV and the client in C-band

Feed	11.45 GHz	11.61 GHz	11.77 GHz	11.93 GHz	12.09 GHz	12.25 GHz
2	-91.888	-93.391	-94.324	-92.881	-92.659	-94.362
4	-140.371	-141.774	-141.761	-143.039	-144.2532	-142.045

Table 4.2: The coupling coefficients in dBW of the interactions between the MEV and the client in Ku-band

C-band and Ku-band using both feed 2 and feed 4 as receivers.

At first glance, these numbers look like good news, as they are generally rather low, meaning that the MEV should be safe to transmit during its mission operations. This may very well be true, but these numbers also lack important context which holds much more information about the safety of the mission as a whole. Notably, these values are also the end values for the approach scenario, described in detail in Section 4.1.2. That scenario and the following ones in Sections 4.1.3 and 4.1.4 provide a much clearer picture of the coupling potential over the entire mission, and show that there is much more to the story than what is presented in Tables 4.1 and 4.2.

4.1.2 Approach

Figure 4-1 shows the results of the first two scenarios featuring the MEV model. Both show coupling between the MEV's TCR boom and the client's feed 2 with the MEV starting exactly 200 m above the client and then moving vertically downward until it finally docks with the client. In the plot to the left, levels begin between -90 to -85 dBW, and steadily increase as the MEV gets closer to the client, which is to be expected. The unexpected result here is that the coupling actually reaches its peak level 5 to 10 meters above the client, rather than when it is docked. This level, at approximately -55 dBW, is the highest seen out of all scenarios. When the MEV gets

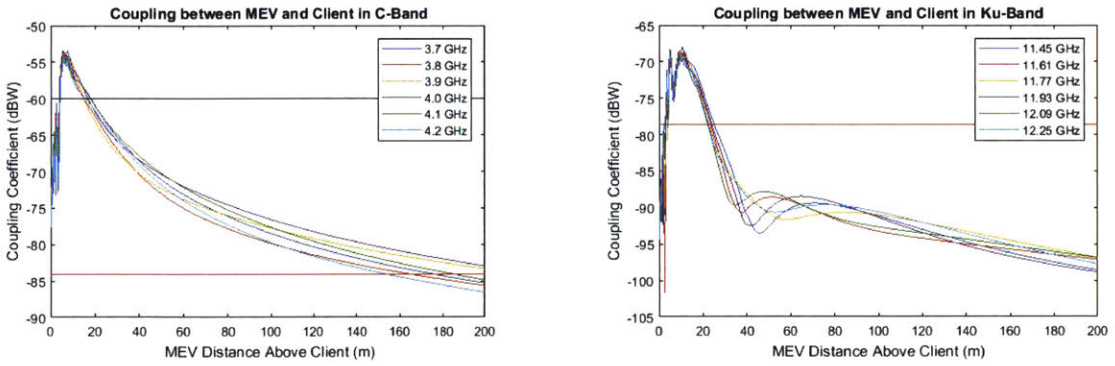

(a) (b)

Figure 4-1: The coupling level in dBW between the MEV and the client's feed 2 in C-band (left) and Ku-band (right). The red horizontal line represents the approximate threshold for interference while the black line is the approximate threshold for damage.

closer than 5 m, the coupling drops by about 15 to 20 dB, down to the levels seen in the docked scenario. This plot was produced using the default polarizations for the MEV and the client, with the MEV using RHCP and the client using linear x polarization. The highest coupling level seen overall is -53.352 dBW, at 3.7 GHz at a distance of 5.5 m above the client.

Table 4.3 shows the coupling coefficient at this same distance and frequency for different polarizations used by the transmitter and receiver. It shows that when the transmitter is using circular polarization, the coupling into a receiver using linear polarizations is roughly the same, and is about 3 dB lower than if the receiver matched the polarization of the transmitter. If the transmitter and receiver are using opposite circular polarizations, however, the coupling coefficient drops significantly, down 25 dB or more from its maximum levels. This case also showcases some of the variability

		Receiver Polarization			
		Linear x	**Linear y**	**RHCP**	**LHCP**
Transmitter Polarization	**RHCP**	-53.352	-53.610	-50.470	-85.101
	LHCP	-53.517	-53.051	-75.208	-50.281

Table 4.3: The variation in the coupling coefficient that results from varying the polarization in the transmitter on the MEV and the receiver on the client. Numbers are calculated at 3.7 GHz, with the MEV 5.5 m above the client and feed 2 as the receiver.

due to the angle of feed 2, as the coupling level is 10 dB lower when the MEV is using LHCP and the client is using RHCP than when their polarizations are reversed. Another interesting note which is not shown in the table, is that for all polarization combinations, 3.7 GHz still exhibits the highest coupling level among the sample frequencies, except for the case of mismatched circular polarizations, in which the coupling levels are more variable and it is actually among the lowest. This trend is seen in all other scenarios as well. As shown by Table 4.3, the highest overall level of coupling seen throughout all scenarios is -50.281 dBW, at 3.7 GHz, 5.5 m above the client, and with both satellites using LHCP. Notably, this level is above the thresholds for both interference and damage, and Chapter 5 discusses exactly how problematic this result is.

In the plot to the right (Figure 4-1b), many of the same patterns are observed, with slight differences. This is the output of the same scenario, but in Ku-band rather than C-band. Here, the coupling rises steadily for the first 120 m or so, then experiences some small fluctuations before a steep increase in coupling levels from 40 m to 10 m above the client. This is in contrast with the C-band results, in which the levels and rate of change both increased up to the peak, but did so in a much more smooth and continuous way. There is a peak around 10 m above the client, with a small drop off and then another peak at a distance of 5 m. The levels then drop off about 20 dB as the MEV reaches its docked configuration, consistent with both the docked scenario and the C-band results. The magnitude of the coupling in Ku-band is notably much lower than in C-band; the peak, while being similar in location, is 25 dB less than in the C-band case. The reasoning for this can be seen in the equations used to calculate the coupling, which include a λ^2 term, meaning that the coupling should increase as the wavelength increases. As both of the plots show, there is variation in the coupling levels even with the frequencies within each band, revealing some nuance in this interpretation, but it can still be shown to work over large frequency differences such as different bands.

The polarization analysis showed similar results in Ku-band as in C-band; the coupling levels are essentially even when the client used linear polarization, are slightly

		Receiver Polarization			
		Linear x	**Linear y**	**RHCP**	**LHCP**
Transmitter Polarization	**RHCP**	-67.977	-68.010	-64.983	-114.881
	LHCP	-68.042	-68.147	-109.027	-65.084

Table 4.4: The variation in the coupling coefficient that results from varying the polarization in the transmitter on the MEV and the receiver on the client. Numbers are calculated at 11.45 GHz, with the MEV 10.5 m above the client and feed 2 as the receiver.

higher when it matched the MEV's circular polarization, and are much lower when using the opposite circular polarization. The main difference is that the levels for all polarization combinations are about 15 dB lower in Ku-band than in C-band, with the exception of the mismatched circular polarizations, which are 30 to 35 dB lower than in C-band. The numbers in Table 4.4 are for the location with the highest coupling, 10.5 m above the client, at the frequency with the highest coupling coefficient at that point, 11.45 GHz. It shows that the highest Ku-band coupling for the overall scenario is -64.983 dBW when both satellites are using RHCP.

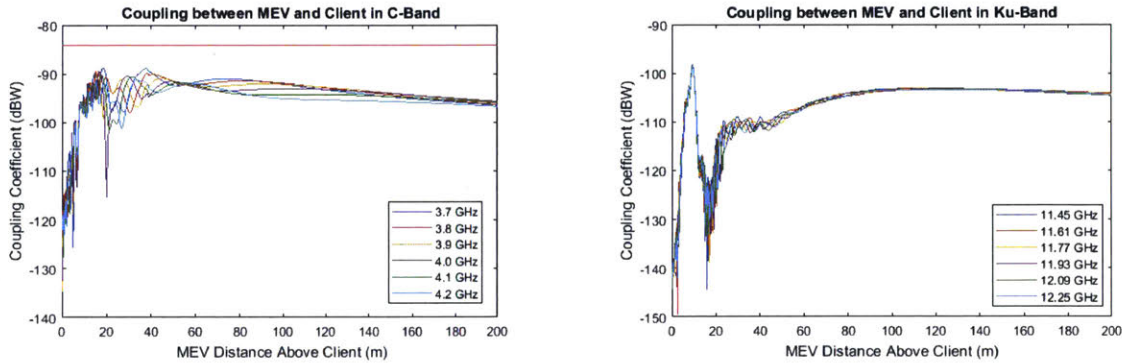

(a) (b)

Figure 4-2: The coupling level in dBW between the MEV and the client's feed 4 in C-band (left) and Ku-band (right). The red horizontal line represents the approximate threshold for interference.

Figure 4-2 shows the results of the same scenario using feed 4 as the receiver rather than feed 2. A key difference between these two feeds, highlighted in Figure 3-8, is that feed 2 is slightly offset from the MEV transmitter's boresight but is pointing largely upwards, while feed 4 is located on the same x-y diagonal as the TCR boom,

but it is angled away from the transmitters. This puts the MEV in a different portion of feed 4's pattern than it is in with respect to feed 2. This leads to a slightly different behavior in the coupling plots. The coupling level remains nearly constant until the MEV is approximately 60 m above the client, with this level being lower than that seen by feed 2 during any point on approach. At a distance of 60 m it can be seen, as suggested by Figure 4-1b, that the coupling numbers start to become more erratic at that point and below. Beyond this, in both cases, there is a small dip in coupling levels before a later spike, which is much more pronounced in Ku-band than it is in C-band. As seen previously, this spike occurs 10-20 m above the client before dropping to much lower levels upon docking, in this case by 30 to 40 dB. Throughout all of this, however, coupling never rises much above -100 dBW in Ku-band and never exceeds -90 dBW in C-band and is therefore less of a risk to feed 4 than feed 2 in this scenario.

The peak coupling level in C-band for this scenario is at 18.5 m above the client, again at 3.7 GHz, the lowest frequency used. Table 4.5 shows the variation in coupling at this location and frequency with polarization with respect to the transmitter and receiver. A different behavior can be seen here than is seen with feed 2. There is greater variability in the coupling from transmitters with circular polarizations to receivers with linear ones. The table also shows that the combinations with matching circular polarizations actually exhibit lower coupling coefficients than combinations with opposite circular polarizations. The reasons for this are complicated, but it seems to be caused by scattering effects when the MEV gets close to the client. As can be seen in Figure 4-2a, there is a great deal of variability in the coupling level between

		Receiver Polarization			
		Linear x	**Linear y**	**RHCP**	**LHCP**
Transmitter Polarization	**RHCP**	-88.709	-86.984	-99.138	-84.913
	LHCP	-86.202	-90.543	-85.156	-96.402

Table 4.5: The variation in the coupling coefficient that results from varying the polarization in the transmitter on the MEV and the receiver on the client. Numbers are calculated at 3.7 GHz, with the MEV 18.5 m above the client and feed 4 as the receiver.

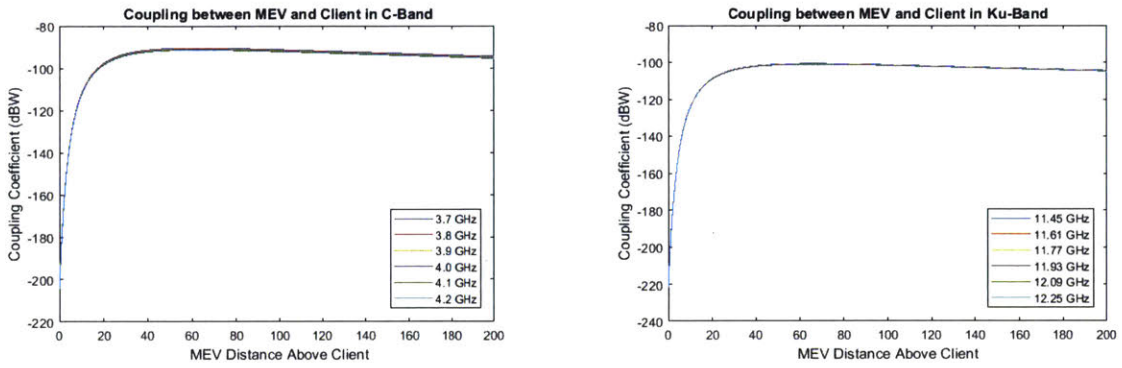

(a) (b)

Figure 4-3: The same scenario shown in Figure 4-2 with all scattering surfaces removed from analysis. This shows that many of the features in those plots as well as the spike in Figure 4-2b are caused by scattering.

frequencies, especially when the two spacecraft are close to each other. This variability is a direct result of scattering off of the client bus, and is eliminated when the scenario is rerun without scatterers considered (i.e. direct feed to feed coupling) as shown in Figure 4-3. The variability between frequencies is also present in the polarization analysis. Unlike in the previous two plots where the peak coupling occurred at a rather specific spot at which the frequencies are grouped closely together, Figure 4-2a shows that the peak is much less clearly defined and that the coupling can take a range of values at many points depending on frequency. It is then this same effect which causes variability in the coupling due to different polarization combinations, and this also seems to be the reason for the deviation from the intuitive pattern seen in Tables 4.3 and 4.4. Here the highest coupling level seen is -84.913 dBW, but the high variability casts doubt on whether this is the overall highest value without running the scenario eight times with all polarizations. It does, however, provide a good order of magnitude estimate for the peak coupling in the scenario.

The peak coupling level in Ku-band is at 9.5 m, and is again at 11.45 GHz, the lowest frequency in the Ku space-to-Earth band. The patterns exhibited in this case are different from the other cases seen thus far. This case continues the trend seen in the previous scenario in which the matched circular polarizations exhibit lower coupling than the opposing ones, although the gap between the two is lower here. It

		Receiver Polarization			
		Linear x	**Linear y**	**RHCP**	**LHCP**
Transmitter Polarization	**RHCP**	-98.117	-106.350	-104.959	-98.370
	LHCP	-97.639	-112.021	-99.831	-101.276

Table 4.6: The variation in the coupling coefficient that results from varying the polarization in the transmitter on the MEV and the receiver on the client. Numbers are calculated at 11.45 GHz, with the MEV 9.5 m above the client and feed 4 as the receiver.

again showcases the effect of scattering on the polarization analysis, as a circularly polarized wave that is reflected off of a surface changes its direction of propagation but not its direction of rotation, effectively reversing its polarization. [17] At first glance, Figure 4-2b seems to show a tight peak like the two plots in Figure 4-1. However, that peak is a direct result of scattering, and does not appear when direct feed to feed coupling is calculated. When no scattering surfaces are included in the analysis, the coupling begins much as it does in Figure 4-2b, but begins to decrease sharply as it gets closer. The deviation due to scattering begins around 60 m above the client. As the sharp peak is caused entirely by scattering, these effects are also shown in the polarization analysis in Table 4.6. The table shows that the coupling into feed 4 is much higher when it is using linear x polarization than linear y, suggesting that the scattering may have a different effect on different polarizations, and if the client had been using linear y polarization, the peak might not even be there. It also shows the same situation as the previous one in which mismatched circular polarizations led to higher coupling than matched ones. The highest coupling value seen in this analysis is -97.639 dBW, and unlike the previous case in which the peak value is in question, the peak value in this case came from a sharp, well-defined peak in the plot, suggesting that this actually is the highest value overall, even if that peak is caused by scattering.

As an illustration, Table 4.7 shows the same scenario run at 100 m above the client rather than 9.5 m, and it features a return to the same patterns observed in the first two polarization analyses. The coupling is roughly the same when the client is using linear polarization, is approximately 3 dB higher when the polarizations are

		Receiver Polarization			
		Linear x	**Linear y**	**RHCP**	**LHCP**
Transmitter Polarization	**RHCP**	-103.229	-103.545	-100.391	-124.383
	LHCP	-103.200	-103.482	-125.379	-100.342

Table 4.7: The variation in the coupling coefficient that results from varying the polarization in the transmitter on the MEV and the receiver on the client. Numbers are calculated at 11.45 GHz, with the MEV 100 m above the client and feed 4 as the receiver.

matched, and about 25 dB below that when they are opposing. This shows that when scattering is not the dominant factor and when the coupling is roughly equal for all frequencies within a band, this pattern can be assumed to hold.

Now that a pattern has been observed for situations with low intra-band variability, this result can be extrapolated to other scenarios that meet the same criteria. In these cases, it is now known how different polarization combinations affects the overall coupling level, and the maximum level can be approximately determined by the result of the default combination of RHCP on the transmitter and linear x on the receiver. For situations with high intra-band variability and a high degree of scattering effects, the results of the polarization analyses are too variable to be demonstrative of anything but their exact geometry. Even a full polarization analysis at a peak from one polarization combination may not give the true highest value, and even if such a value is found, the generic nature of the servicer and client models would make such a result inapplicable to any real world scenario involving different geometries and many more scattering surfaces. Thus, the polarization analysis method performed at the peak in the plot for the default combination can serve as an order of magnitude estimate for coupling in that situation, as opposed to a more exact result. As such, further polarization analyses are not shown, but the highest value obtained from them is still reported.

4.1.3 y-axis Flyover

The results of the second MEV scenario are shown in Figure 4-4. In this scenario, the MEV maintained a relative distance above the client of 100 m in the +z direction

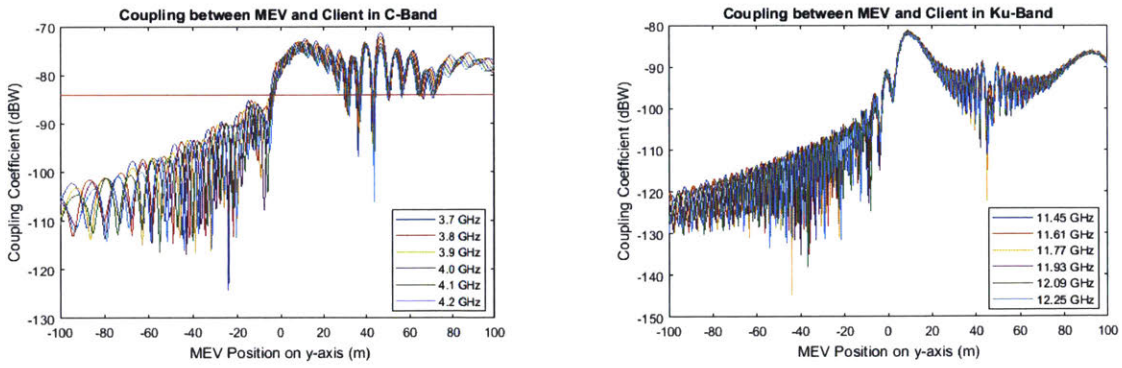

(a) (b)

Figure 4-4: The coupling level in dBW between the MEV and the client's feed 2 in C-band (left) and Ku-band (right). The red horizontal line represents the approximate threshold for interference.

while moving laterally in the +y direction starting at y = -100 and ending at y = 100. The axes are as denoted in Figure 3-12. It should be noted for reference that feed 2 on the client is located on the +y panel of the bus, while feed 4 is located underneath the +x +y corner of the bus. Figure 4-4 shows the results for feed 2. Since this feed is located on the client's +y bus panel, the bus effectively shadows it from the transmitter on the MEV whenever it is on the opposite side of the client. This is seen in the low coupling numbers for the range of y = -100 to y = 0 in the plots, which rise steadily as the MEV gets closer but stay below roughly -90 dBW for C-band and -100 dBW for Ku-band. From y = 0 to y = 100, levels are higher, as one would expect since the feed is no longer shadowed, and the coupling pattern follows the rough pattern of the sidebands of the client's antenna.

The two spacecraft are separated by at least 100 m at all times, scattering effects are not a dominant factor in the coupling in this scenario. Using a diameter of 1.5 m for the receive antenna and 0.1 m for the transmit antenna, Equation (2.10) shows that the Fraunhofer distance in C-band is about 68 m, while in Ku-band it is 204 m. Thus, feed 2 is in the near field of the MEV for the entirety of this scenario in Ku-band, but it is in the far-field in C-band. Even with this distinction, the results in the two frequencies are rather similar, and the intra-band variability is actually lower in Ku-band even though the coupling is done in the near-field. An analysis of the

polarizations used on the transmitter and receiver shows roughly the same pattern discovered previously for low scattering cases. The variability between frequencies is high in much of both of these plots, however, and a polarization analysis done in C-band shows that this variability between frequencies is still present when using other polarizations, but it is much more predictable. The coupling gradually decreases as the frequency is increased, and the far-field polarization effects are seen within each frequency individually as well. Peak coupling in this case is -69.661 dBW for C-band and -78.191 dBW for Ku-band, with both spacecraft using RHCP in both cases, although the coupling values for LHCP are not far off.

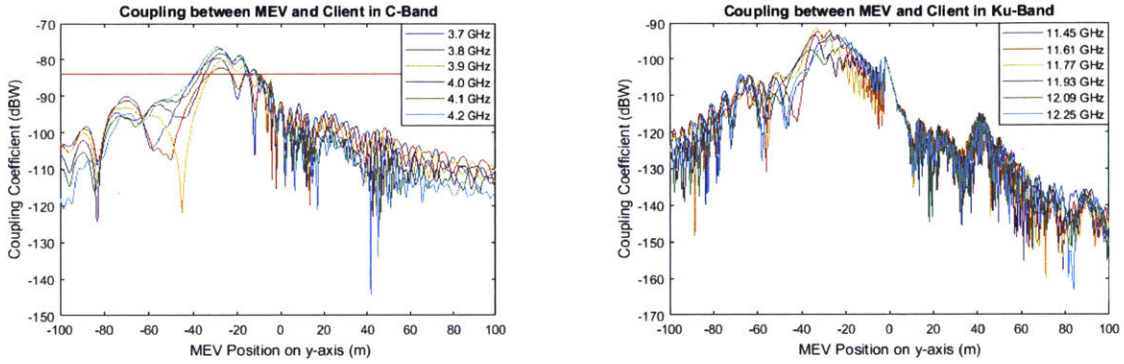

(a) (b)

Figure 4-5: The coupling level in dBW between the MEV and the client's feed 4 in C-band (left) and Ku-band (right). The red horizontal line represents the approximate threshold for interference.

Figure 4-5 again shows the results of the y-axis flyover scenario, but with coupling calculated into feed 4 instead. A pattern is not as easy to make out here, but due to shadowing from the client bus, the feed should not have a direct line of sight to the MEV TCR boom until about y = +14. Even after this, the feed is angled slightly in the -y direction toward its reflector, so it does not do an effective job of collecting radiation from the MEV. Still, the relatively slow rate of change when the MEV is on the -y side of the client is consistent with the transmitter being blocked, while the rising coupling coefficient as the MEV approaches y = 0 is consistent with the radiation that is getting through being stronger due to a closer proximity to its source. The shadowing and angling lead to a high degree of variability in the coupling

coefficient between frequencies in both C-band and Ku-band. A polarization analysis finds that this variability leads to large inter-frequency differences in this manner as well, although being in the far-field does keep the intra-frequency variation to what would be expected. Coupling in this case peaks at -75.278 dBW in C-band and -91.470 dBW in Ku-band, with both spacecraft using LHCP.

4.1.4 x-axis Flyover

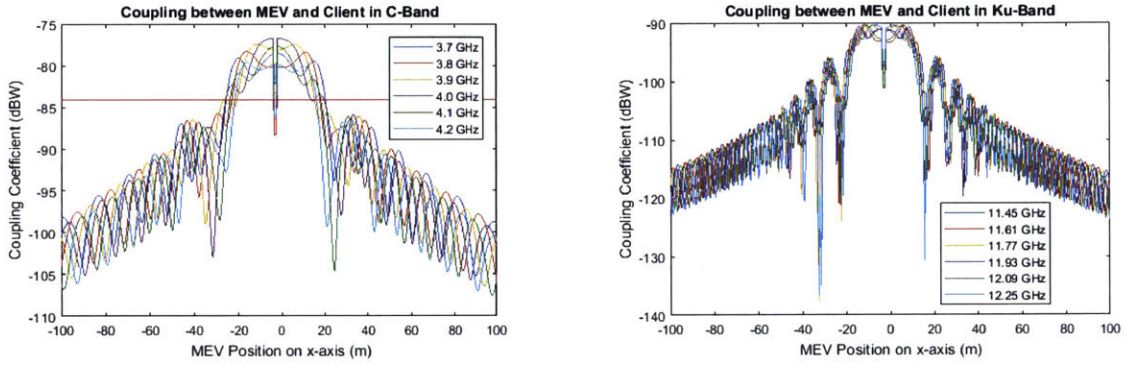

(a) (b)

Figure 4-6: The coupling level in dBW between the MEV and the client's feed 2 in C-band (left) and Ku-band (right). The red horizontal line represents the approximate threshold for interference.

This scenario is similar to the last except that the MEV is traveling along the x-axis rather than the y-axis. This changes the geometry slightly, such that feed 2 on the client is no longer shadowed in the first half of the scenario. In fact, with the TCR boom extending out 3 meters in the +x and +y directions in the MEV coordinate system, the only time that feed 2 is shadowed in the entire scenario is in the center, when its line of sight to the boom is blocked by its own reflector. This can be seen in Figure 4-6, as the coupling coefficients neatly follow the antenna pattern of the feed-reflector system. Both plots show peaks in the center (at y = -3, as the overall MEV coordinate system is what is being moved, and the TCR boom is 3 m offset from this), surrounded by symmetric sidelobes that decrease in magnitude as the distance from y = -3 increases. The highest level of coupling seen in C-band is at this peak, coming out to -73.966 dBW when both spacecraft are using LHCP. The maximum

Ku-band coupling is in the same location, and is -87.434 dBW when both are using RHCP. This case in particular showcases that, holding all else equal, increasing the frequency decreases coupling, as shown by the $\frac{\lambda^2}{4\pi}$ terms in equations (2.7) and (2.26).

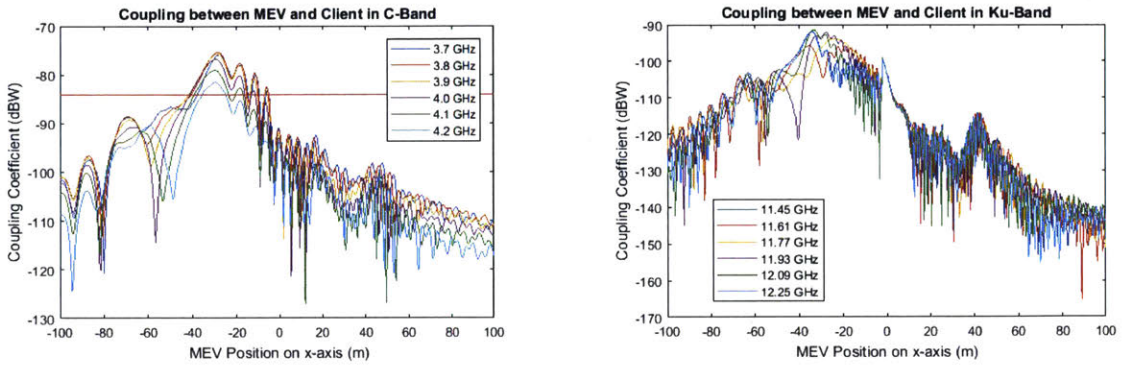

(a) (b)

Figure 4-7: The coupling level in dBW between the MEV and the client's feed 2 in C-band (left) and Ku-band (right). The red horizontal line represents the approximate threshold for interference.

Figure 4-7 shows the results for the x-axis Flyover scenario with feed 4 as the receiver. In this case, as the feed's location and orientation on the x-axis are the same as on the y-axis; the geometry for this scenario did not turn out to be all that different than the previous scenario. This is seen in the striking similarity between Figure 4-7 and Figure 4-5. The same shadowing and angle effects are observed, and the overall peak coupling levels remain similar. The same amount of intra-frequency variability of the coupling levels can also be seen in this scenario as well. These levels are -75.186 dBW in C-band and -92.325 dBW in Ku-band, with both satellites using RHCP in both cases.

4.2 RSGS Results

4.2.1 Docked

The docked scenario for RSGS serves both as a way to calculate the level of RF coupling seen during the servicing operations phase of its CONOPS and as a way to validate the computational strategy used to run all subsequent scenarios in a

Frequency (GHz)	11.45	11.61	11.77	11.93	12.09	12.25
Coupling Coefficient (dBW)	-124.310	-122.380	-119.256	-119.240	-122.199	-122.340

Table 4.8: Coupling levels from the RSV into the client's feed 2 while grappled to the client (High Fidelity)

Frequency (GHz)	11.45	11.61	11.77	11.93	12.09	12.25
Coupling Coefficient (dBW)	-125.496	-123.724	-118.875	-118.437	-120.980	-121.221

Table 4.9: Coupling levels from the RSV into the client's feed 2 while grappled to the client (Low Fidelity)

reasonable amount of time. In Tables 4.8 and 4.9, the results of the docked scenario are shown in both "high fidelity" and "low fidelity." The former describes the scenario in which ray output on the RSV's reflector is set to all, which leads to runtimes of several hours for calculating currents on each of the subsequent surfaces. The latter describes the scenario in which the ray output on the RSV's reflector is set to none and the rest of the currents are calculated from that, and the coupling from the reflector is calculated separately and added in later.

These results show that the difference between the two methods of calculating coupling is not large. In fact, the low fidelity coupling values are all lower than the high fidelity values by no more than 2 dB, a consistent result across all frequencies. This allowed for the use of the low fidelity technique in the other RSGS scenarios by showing that the values output would only be off by a slight amount. It should also be noted that the docked scenario is calculated only for feed 2. As the polarization analysis for the approach scenario shows, this is not necessarily the maximum coupling that would be seen by the client when the RSV is grappled to it.

4.2.2 Approach

Figure 4-8 shows the coupling values as the RSV approaches the client from above, starting at a distance of 200 m, similar to the MEV scenario. The plots showcase the effect of the highly directional reflector antenna used on RSGS versus the hemispheri-

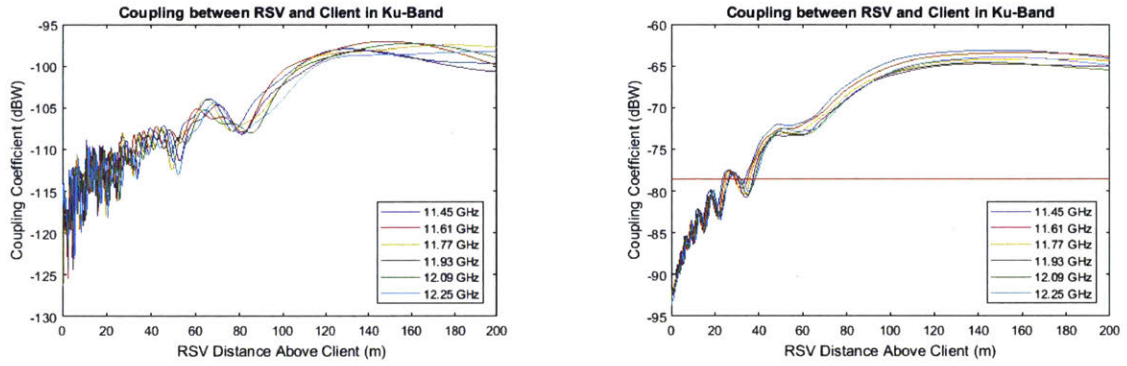

(a) (b)

Figure 4-8: The coupling level in dBW between the RSV and the client's feed 2 (left) and feed 4 (right) in Ku-band. The red horizontal line represents the approximate threshold for interference. The threshold for damage is at the top edge of the plot for feed 4 at -60 dBW.

cal antenna used on the MEV. Instead of the coupling increasing as one would expect when two antennas move closer to one another, the coupling decreases as a result of the receivers moving further into the sidebands of the RSV's antenna pattern. The sidebands can even be seen on the plot as successive peaks and troughs as the RSV gets closer, though they are much clearer in the plot for feed 4 than the plot for feed 2. The rate movement through the sidebands increases as the distance between the two spacecraft decreases because the slight offset of the transmitter from the receivers in both the x and y directions leads to a greater relative angular velocity between the two when they are close. Thus, the coupling coefficient starts out high in both cases when the receivers are in the main beam of the transmit antenna and gradually decreases as the beamwidth of the antenna decreases due to a closer distance.

While the two plots appear similar in shape with the exception of increased noise and variability when the RSV gets close to feed 2, they differ greatly in their magnitudes. The coupling into feed 4 peaks at around -65 dBW, while the coupling into feed 2 peaks at less than -95 dBW. This is where the polarizations and geometry of the transmitter and receivers begins to take on a much greater importance. Both the RSV and the client are using linear x polarization for this scenario, but the coordinate system for feed 2 is at a 90 degree angle to the RSV transmitter's coordinate system, and feed 4's coordinate system is at a 45 degree angle to both. Table 4.10

		Receiver Polarization			
		Linear x	**Linear y**	**RHCP**	**LHCP**
Transmitter Polarization	**linear x**	-98.603	-69.033	-71.774	-72.321
	linear y	-68.705	-100.186	-71.501	71.934
	RHCP	-71.989	-72.269	-90.450	-69.148
	LHCP	-71.450	-71.801	-68.634	-91.452

Table 4.10: The variation in the coupling coefficient that results from varying the polarization in the transmitter on the RSV and the receiver on the client. Numbers are calculated at 11.45 GHz, with the RSV 150 m above the client and feed 2 as the receiver.

		Receiver Polarization			
		Linear x	**Linear y**	**RHCP**	**LHCP**
Transmitter Polarization	**linear x**	-62.987	-62.780	-62.679	-63.096
	linear y	-60.714	-60.649	-60.708	-60.655
	RHCP	-61.988	-61.460	-76.975	-58.771
	LHCP	-61.393	-61.743	-58.638	-75.759

Table 4.11: The variation in the coupling coefficient that results from varying the polarization in the transmitter on the RSV and the receiver on the client. Numbers are calculated at 11.45 GHz, with the RSV 150 m above the client and feed 4 as the receiver.

shows how the coupling coefficient changes when different polarizations are used on the transmitter and feed 2, while Table 4.11 does the same for feed 4. As the coupling is highest when the RSV is higher above the client, these values are calculated at a point when both feeds are clearly in the transmit antenna's main beam, at 150 m above the client. The 90 degree offset between the transmitter and feed 2 leads to an apparent shift of the polarization from horizontal to vertical from the point of view of feed 2, leading to vastly reduced coupling when both are set to the same linear polarization. However, when one is set to linear x and the other to linear y (or vice versa), their polarizations actually line up, and the coupling increases. With feed 4 being at a 45 degree angle to the transmit antenna, both forms of linear polarization have the same effect on it. Both feeds exhibit the same behavior seen in the MEV scenarios with regard to interactions between circular and linear polarizations; these levels are approximately 3 dB lower than those with matched polarizations.

The other interesting feature here is that the coupling for matched circular polar-

izations is lower than that for opposite circular polarizations. This can be attributed to the reflector on the RSV; the direction of rotation of the polarization vector of the transmitted wave remains the same when it hits the reflector, but its direction of propagation is reversed, effectively turning a right-hand circularly polarized wave into a left-hand circularly polarized wave (and vice versa). Normally, there would be a reflector on the receive side to reverse the polarization again, but in this case the coupling is unintended and has a direct path from the transmit reflector to the receive feed. Thus, a wave transmitted with RHCP is propagated as an LHCP wave, and therefore produces higher coupling in a receiver tuned to LHCP. [17] All of these trends are seen in the polarization analyses for the other scenarios, so the full results of those analyses are not shown, but notable values are still reported.

The highest coupling value seen in the approach scenario is -58.638 dBW with the RSV using LHCP and feed 4 using RHCP, and this level is close to that seen when the two polarizations are reversed. In general, the coupling between the RSV and feed 4 is about 10 dB higher than coupling between the RSV and feed 2 for corresponding polarization combinations. This can be attributed to the fact that feed 4 is closer to the center of the RSV's transmit beam than feed 2 is. This also manifests itself in the fact that feed 2 leaves the main lobe of the transmit antenna pattern at a greater height than feed 4, as showcased by the first minor peak in Figure 4-8a occurring at around 70 m compared to the first minor peak in Figure 4-8b occurring at approximately 50 m.

4.2.3 y-axis Flyover

In this scenario, the RSV moves along the y axis while staying 100 m above the client in the z direction the entire time. Figure 4-9a shows the coupling into feed 2 and Figure 4-9b shows the same into feed 4. Feed 2 is shadowed by the client bus when the RSV is on the -y side of the client, but moves into view in the other half of the scenario, after which the coupling values begin to oscillate rapidly as the two antennas move through each others' sidelobes and decreases as the distance between the satellite increases. Feed 4 is not shadowed at any point during the scenario, but

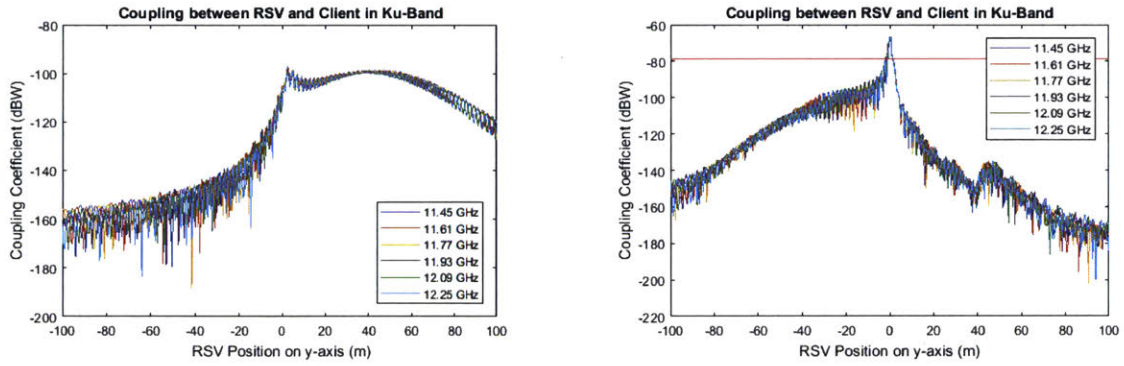

(a) (b)

Figure 4-9: The coupling level in dBW between the RSV and the client's feed 2 (left) and feed 4 (right) in Ku-band. The red horizontal line represents the approximate threshold for interference. The threshold for damage is at the top edge of the plot for feed 4 at -60 dBW.

its angle toward the -y direction gives the appearance of skewing the coupling values in that direction. The peaks in both scenarios come as the RSV is nearly directly overhead, again showing the effect of the increased directivity of the transmit antenna on the RSV compared with that on the MEV. The highest coupling level into feed 2 is -74.291 dBW when the RSV is using RHCP and the client is using LHCP, while the highest coupling seen by feed 4 is -62.834 dBW with the client and RSV polarizations reversed.

4.2.4 x-axis Flyover

Figure 4-10 shows the results of the RSV traveling along the x-axis rather than the y-axis. This time feed 2 is not shadowed at all, and the coupling is symmetric around x = -2, when the RSV's reflector is directly overhead. Because the location and orientation of feed 4 are the same in the x and y directions, its plot looks largely as it did for the y-axis flyover scenario with some minor differences. Both plots include a large peak in the middle while the feeds are within the RSV antenna's main beam, with a 20 to 30 dB drop in coupling within a few meters of passing overhead. The highest level of coupling into feed 2 is -60.902 dBW when the RSV is using LHCP and feed 2 is using RHCP, while the highest coupling into feed 4 is -62.595 dBW using the

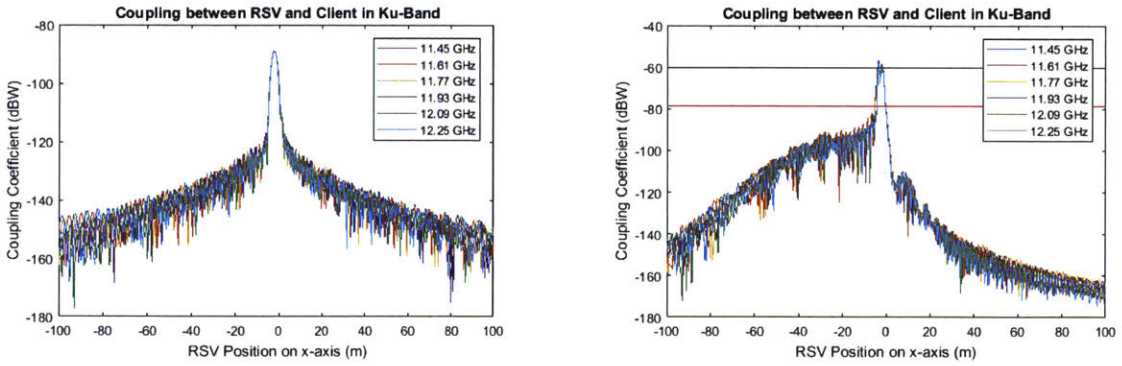

(a) (b)

Figure 4-10: The coupling level in dBW between the RSV and the client's feed 2 (left) and feed 4 (right) in Ku-band. The red horizontal line represents the approximate threshold for interference while the black line is the approximate threshold for damage.

same polarization combination. This is a notable result because the variation in the RSV's x coordinate allowed feed 2 to get deeper into the transmit antenna's pattern than it had been before, verifying that this is the reason it had seen lower coupling than feed 4 in previous scenarios. With this constraint removed, it ultimately has a slightly higher coupling level than feed 4.

4.2.5 Inspection

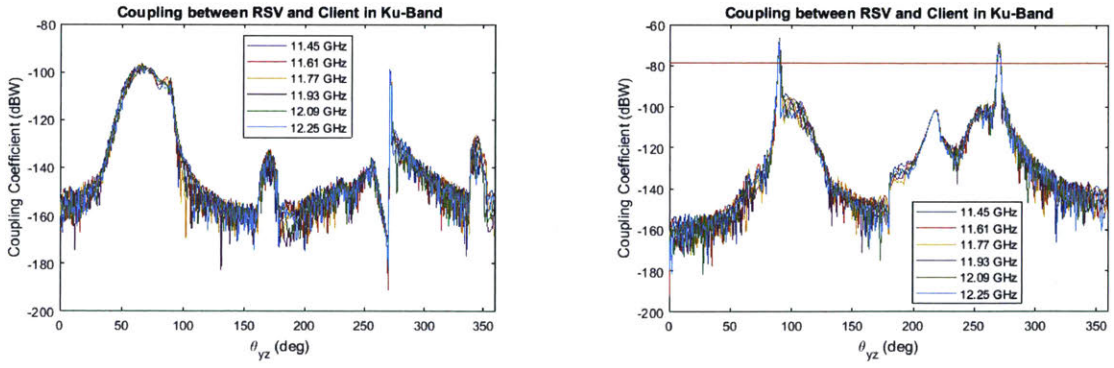

(a) (b)

Figure 4-11: The coupling level in dBW between the RSV and the client's feed 2 (left) and feed 4 (right) in Ku-band. The red horizontal line represents the approximate threshold for interference. The threshold for damage is at the top edge of the plot for feed 4 at -60 dBW.

This scenario is different from any of those done for the MEV or the previous ones done for RSGS. It drew its inspiration from the inspection portion of the RSGS CONOPS, and saw the RSV circling around the client at a distance of 100 m while still pointed downward as if it is communicating with its MOC on the ground. Figure 4-11 shows the results of the RSV rotating about the x-axis, varying its position in the y and z directions. It begins on the +y-axis (0 degrees) and begins to move up toward the +z-axis (90 degrees) before moving down again toward the -y-axis (180 degrees) and then the -z-axis (270 degrees) before coming back to the +y-axis. These plots show new features at different angles that had not been explored previously. Figure 4-11a shows a broad peak from about 50 degrees to 90 degrees in which the RSV travels through a backlobe of the reflector. It also shows two small peaks, one just before 180 degrees and the other just before 360 degrees. It also shows coupling decreasing steadily as the RSV approaches the 270 degree point, and then rise dramatically to a peak. This is due to the portion of the scenario just before 270 degrees, when the reflector being fed by feed 2 is shadowed from the RSV by the client bus. Radiation collected by the reflector and sent into the feed is a major contributor to the overall coupling coefficient; it being shadowed drives the coupling down, and when it comes back into view, especially as the RSV is right below the client, it drives the coupling back up.

Figure 4-11b shows the same scenario with coupling calculated into feed 4. It shows two clear, narrow peaks at 90 degrees and 270 degrees, corresponding to when the RSV is directly above and directly below the client. There is also a smaller peak at about 220 degrees, possibly from interactions with one or more of the four reflectors on the bottom of the client bus. This plot, even more so than the other, is demonstrative in pointing out where the problem points are for a servicer. Coupling is highest when the servicer is above and below its client using this feed configuration, with large drop offs anywhere else, although there may be smaller peaks at other points.

The peak coupling level into feed 2 is -79.430 dBW when the RSV is 66 degrees above the +y-axis, and when it is using RHCP and feed 2 is using LHCP. The highest

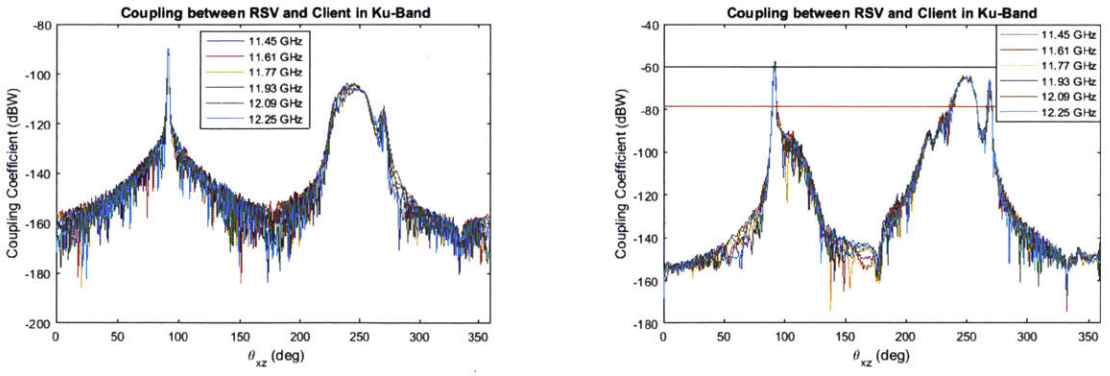

(a) (b)

Figure 4-12: The coupling level in dBW between the RSV and the client's feed 2 (left) and feed 4 (right) in Ku-band. The red horizontal line represents the approximate threshold for interference while the black line is the approximate threshold for damage.

coupling level into feed 4 is -62.719 dBW when the RSV is directly above the client, and with the polarizations reversed. The discrepancy between the maximum coupling into feeds 2 and 4 is again explained by the RSV only moving in the y and z directions, placing feed 4 further into its transmit pattern than feed 2.

Figure 4-12 shows the results of the same scenario, except with the RSV making a revolution about the y-axis rather than the x-axis. In this case, feed 2 does not have the same shadowing issues that it doeswhen revolving around the x-axis, leading to an overall smoother plot with only two peaks. The first is tall and narrow, consistent with others seen when the RSV is above or below the client. The other is not quite as tall, and is much wider, suggesting that feed 2 passes into a backlobe of the RSV's transmit antenna. The maximum coupling seen by feed 2 in this case is -61.606 dBW at 1 degree past the +z axis, when the RSV's reflector is closest to being directly overhead.

The plot for feed 4 looks very similar, with a narrow peak at 90 degrees and another wide peak around 250 degrees. This plot includes a separate peak at 270 degrees which is due to the RSV being directly beneath the client, while the wider one is presumably due to the effect of the backlobe that caused a similar wide peak for feed 2. The maximum coupling seen by feed 4 in this scenario is -53.906 dBW, again at the same position as the maximum coupling into feed 2.

Chapter 5

Discussion and Conclusion

5.1 Discussion

Each scenario described in Chapter 4 tests a different aspect of the servicing CONOPS and looks at the effects of relative satellite position, transmitter type, receiver location, frequency, and polarization. These variations in different parameters paint a picture of what increases and decreases the level of coupling in order to determine ways to keep unintended coupling to a minimum. The following summarizes the effects of each of them:

- **Frequency** – As suggested by Equations (2.7) and (2.26), an increase in the wavelength, and therefore a decrease in the frequency, of a transmitted wave increases the power coupled into the receiver. This is largely confirmed by the MEV scenarios, in which each scenario is run twice and only this parameter is varied. Coupling in C-band is on average 10 to 15 dB higher than in Ku-band. As shown in the plots for many of the scenarios, this inverse relationship between frequency and coupling is not a strict one, as the coupling level can vary greatly within a band, with some frequencies leading to higher coupling in some areas than others depending on the exact scattering geometry at a given point in space and time. This is also seen in the polarization analyses, as when there is a high degree of scattering effects, the difference in coupling between

frequencies for the same polarization combination appears somewhat random, but when these effects are reduced, the coupling returns to the expected pattern of decreasing with increased frequency.

- **Polarization** – The way that polarization is defined in GRASP makes it somewhat more difficult to understand the effect polarization has on coupling, but the polarization analyses done with the coupling scenarios help to make that effect more clear. Despite the appearance of some mismatched polarizations leading to higher coupling, a result mostly due to misaligned coordinate systems, the analyses confirm that matched polarizations do in fact lead to higher coupling as one would expect. They also shed light on other aspects of polarization, such as what happens when a linearly polarized system interacts with a circularly polarized system. In this case, the coupling is often about 3 dB lower than in the matched case, a far cry from the 20 to 30 dB lower coupling that arises from interactions between opposite polarizations. With respect to linear polarizations however, the analyses do showcase how easily they can become misaligned if a spacecraft is rotated around its z-axis. Coupling seems to be reduced by about 3 dB with a 45 degree offset, as shown by the feed 4 linear polarization results, but the feed 2 results show that by the time the offset hits 90 degrees the coupling has been reduced by tens of dB. With respect to circular polarizations, the analyses highlight the fact that when a reflector antenna is used, the effective polarization is reversed, meaning that just because two systems are designed to use opposite circular polarizations does not mean they are safe from undesired coupling if one or both uses a reflector, and this might even make their risk greater.

- **Transmitter Type** – The analysis done in this thesis really only tests two different types of transmitters, drawn from plans for the MEV and RSGS, but these represent two different classes of antennas. One is a low gain system with a small aperture and a main lobe spread over an entire hemisphere, while the other is a high gain, highly directive, more traditional reflector antenna system.

Overall, the MEV scenarios often have the higher coupling values, although there are some caveats to this. The MEV used C-band, which leads to higher coupling due to frequency, but when a Ku-band comparison is made the MEV still has higher coupling in most cases. This can be attributed to the fact that the wider beam pattern on the MEV leads to a slower angular drop off in gain between the antenna boresight and other areas, so the coupling at other angles far from the boresight is relatively higher than it would be for a high directivity antenna. On the other hand, while the RSGS antenna leads to lower coupling in most cases, it does lead to large spikes in coupling whenever one of the receivers on the client enters its main beam. Even at a distance of 100 m, the levels seen when the receivers are within the main beam are even with or higher than the highest levels seen from the MEV at any point. Because the receivers move out of the main beam as the RSV gets closer to them, there is no estimate of what the coupling might have been if they had stayed within that beam with a smaller separation between them and the transmit antenna, however it is safe to assume that that number would have gotten larger, and that this would have been the largest overall coupling number for all scenarios had it occurred.

- **Receiver Orientation** – Many of the scenarios reveal some nuances in the way the transmitters interact with the two different client feeds even when holding all else equal. The position of each feed determines how far inside the RSV's main beam it is in those scenarios, and a shift of just a meter or two in one direction has a dramatic effect on the coupling seen. The angle at which each feed is positioned also affects the final coupling numbers in a variety of ways. This affects the portion of the receiver antenna pattern that the transmitter is in, which according to the antenna reciprocity theorem has just as much of an effect on the coupling as the portion of the transmitter pattern that the receiver is in, and depending on whether the receive feed is angled toward or away from the transmit antenna, causes the coupling to increase or decrease, respectively. It also interacts with linear polarizations in different ways, as being

at an angle to the linear polarization as defined by the transmit antenna causes reduced coupling based on the size of that angle. At different portions of some scenarios, some of the feeds are also shadowed by the client bus, leading to reduced coupling in those portions of the scenarios.

- **Satellite Position** – Especially as showcased by the RSGS inspection scenarios, the position of the two satellites relative to each other has a great effect on the coupling level. This is mostly due to the position of each satellite in the other's antenna pattern, and since most energy is directed downward in order to communicate with the ground, the natural place for coupling to be the highest is when one satellite is directly over the other. This is confirmed by the results of these simulations, as the approach scenarios have some of the highest coupling levels, and the inspection scenarios show that the coupling levels are highest at exactly these points. There are other factors that contribute to increased coupling, such as backlobes on offset parabolic reflectors, and these are definitely factors that warrant increased attention, but none are as impactful as one satellite being in the main lobe of another. This is an important result as the CONOPS for the MEV and likely RSGS as well calls for approaching and docking with the client from above, as well as holding at waypoints above the client along the way where coupling may be even higher than when the two satellites are docked.

These factors and their interactions are complex, and the only way to know for sure how much energy is coupled into a particular receiver during an actual mission is to simulate it with more accurate models and a higher degree of fidelity than that used here. But the results of the GRASP scenarios show that the servicing missions as planned are going to operate in ways that can increase their risk of a high amount of unintended coupling into their clients' receivers, as well as their own. Both plan on approaching from above, the most dangerous direction in terms of RF coupling, and gradually getting closer while increasing their data rates at precisely that time in order to keep all relevant parties updated on the status of the docking in real time.

Satellite	Scenario	Feed	Band	Maximum Coupling (dBW)
MEV	Approach	2	C	-50.281
			Ku	-64.983
		4	C	-84.913
			Ku	-97.639
	y-axis Flyover	2	C	-69.661
			Ku	-78.191
		4	C	-75.278
			Ku	-91.470
	x-axis Flyover	2	C	-73.966
			Ku	-87.434
		4	C	-75.186
			Ku	-92.325
RSGS	Approach	2	Ku	-68.634
		4		-58.638
	y-axis Flyover	2		-74.291
		4		-62.834
	x-axis Flyover	2		-60.902
		4		-62.595
	y-z Inspection	2		-79.430
		4		-62.719
	x-z Inspection	2		-61.606
		4		-53.906

Table 5.1: The maximum level of coupling seen for each scenario over all positions and polarizations

Before this, both spacecraft will have a phase in which they rendezvous with their client and gather sensor information about it before approaching. In this phase, the relative positions of the satellites can vary greatly, and their relative orientations can potentially open the spacecraft up to higher levels of coupling from the other. RSGS is also planning on doing an inspection of its clients in which it takes imagery at a large number of positions and angles in order to gain a greater awareness of their positions in space. While the RSV will likely not be transmitting and taking images at the same time, the GRASP inspection scenarios outlined the risk to the client if the RSV is transmitting while pointed nadir, and the risk is likely even greater to the RSV if its receiving antennas are pointed at the client while it is inspecting it. All of this is occurring while both the RSV and MEV are operating on similar frequency bands as their clients, creating a greater need for deconfliction just to have signals

from both satellites received properly while also adding much more energy in transmit bands than the client was designed to expect.

Up to this point, this thesis has examined the potential level of RF coupling that can be expected between one of these servicing satellites and its client. Table 5.1 shows the highest levels seen from each scenario, aggregated here for convenience.

These numbers are illustrative of the ways that the satellites interact and how each of the previously mentioned factors changes these interactions, but they do not by themselves show how concerned servicing satellite operators should be about RF coupling. To get an overall picture of the level of risk posed by coupling to servicing missions, these numbers must be put in the context of the level of RF energy normally seen be client receivers and the sensitivity of a typical RF receive chain to increased energy input. This crucial context is explored in Section 5.2.

5.2 Risk Analysis

5.2.1 Interference

In a typical communication link, signal quality is measured using a Signal to Noise Ratio (SNR), comparing the strength of the signal received to that of the noise floor, usually thermal noise combined with other stray energy entering the receiver. An SNR of about 10 dB or greater allows the receiver to distinguish the signal from the noise, while a lower one does not always allow this, and may result in a failure to interpret the signal. Since the energy coupled into the client receivers by a servicer is in a transmit band (3.7-4.2 GHz for C-band or 11.45-12.25 GHz for Ku-band), it will not be mistaken for a signal by the receivers, which are expecting their signals to be in the receive band (5.925-6.425 GHz for C-band or 13.75-14.5 GHz for Ku-band). However, all of this energy is still coupled into the receivers, so it can be modeled as an additional source of noise for the client spacecraft, lowering its overall SNR.

Getting a sense of how RF coupling from a servicing satellite changes the SNR of its client requires first understanding what it would be were the servicer absent.

Any satellite in orbit would already have a detailed link budget completed, outlining how much energy it can expect to receive from its ground station and how much noise it should see as part of normal operations, with a SNR of greater than 10 being one of the prerequisites for even beginning to implement a communication system. However, as this thesis considers a generic client without specific parameters, no such link budget exists; a "generic" link budget must be crafted to match the client model. As the client is well within the far-field of its ground station, Equation (2.7) can help with the signal part of this.

The terms in Equation (2.7) can reasonably take on a great number of values; some simplifying assumptions are used to obtain an order of magnitude estimate for the signal strength seen from GEO. First, the frequencies used are 6 GHz for C-band and 14 GHz for Ku-band. Next, the transmit power for the ground antenna is assumed to be 100 W. [7] The antenna itself is treated as a parabolic reflector with a diameter of 15 m, and assuming GRASP's standard aperture efficiency of $\frac{1}{\sqrt{2}}$. The distance between the two antennas is set to 40,000 km, signifying a transmitter that is not directly underneath the satellite on the equator, but not at the edge of its line of sight either. For this calculation, the client's larger reflector of 1.5 m is used, with its aperture efficiency also assumed to be $\frac{1}{\sqrt{2}}$.

Plugging the antenna diameter, frequency, and efficiency values into Equation (2.6) gives values of 58.0 dBi for C-band and 65.3 dBi for Ku-band for the transmit antenna on the ground and 38.0 dBi for C-band and 45.3 dBi for Ku-band for the receive antenna on the client. The transmit power converted to decibels comes out to 20 dBW, and the path loss comes out to -200.1 dB for C-band and -207.4 dB for Ku-band. Not accounting for any other losses, plugging these numbers into Equation (2.7) gives -84.1 dBW for C-band and -76.8 dBW for Ku-band.

The equation for noise power is given below, where $k_B = 1.38 \times 10^{-23}$ is Boltzmann's constant, T_{sys} is the system noise temperature, and B is the bandwidth of the receiver. As the client's antenna is pointed at the Earth, its noise temperature is assumed to be 290 K, and the bandwidth varies based on the width of the channels used by the client, but a typical channel width would be about 10 MHz. [7] Plugging

these values into Equation (5.1) gives -134.0 dBW.

$$P_N = k_B T_{sys} B \tag{5.1}$$

The first conclusion of note is that the maximum coupling values from every scenario rise well above the noise floor, and even in the scenario with the lowest peak coupling, the addition of typical noise seen by the antenna would only raise that value by about 0.2 dB, meaning that RF coupling from the servicing satellite is the primary source of noise for the client when it is in proximity. The second, and arguably more consequential conclusion is that in many cases the coupling from the servicer can reach levels above the signal that the client is intended to receive. The most extreme case is when the MEV is 5 m above the client and using C-band, when coupling from its transmitter is approximately 45 dB higher than the received signal from the ground.

It is at this point where hardware begins to become a significant factor. A typical RF receive chain consists of the antenna to gather incoming radiation, followed by a Low Noise Amplifier (LNA) to amplify the received signal with a minimal amount of added noise. From there, the amplified signal is mixed with an intermediate frequency signal from a local oscillator to mix it down to a combination of a lower frequency and a higher frequency; the higher one is then filtered out. This is the signal that is then sent as an output for processing or re-transmission, depending on the communication architecture employed by the receiving satellite. Many receivers include a bandpass filter at some point before mixing with the intermediate frequency to ensure that only signals in the desired band are mixed down. If this filter is present, it can attenuate signals in the transmit band by often about 70 to 80 dB. Based on the data produced from the GRASP scenarios, if the energy coupled into the client receiver by the servicer were attenuated by that much, it would be enough to ensure that the intended signal did not get overpowered by transmissions from the servicer. However, without a protective filter, unintended coupling can easily overpower operational signals in certain circumstances. The true level of risk depends on the hardware employed

by the client; with filters with a high amount of attenuation that select only the necessary band and reject all other incoming radiation, coupling from a servicing satellite should not interfere with ordinary operations. Without these measures, the risk is much greater that servicing can cause disruption in the reception of RF signals.

5.2.2 Damage

The threshold for damage is again dependent on the hardware in a given receiver. The component most likely to be damaged is the LNA, and most have a maximum input power listed on their datasheet to signify a level above which they will begin to experience abnormal behavior or potentially damage. The key factor in determining the safety of a given receiver assembly is again the presence of a filter in the RF chain to attenuate signals from the transmit band, but the location of this filter is even more important. In order to protect the LNA, this filter must be placed before it in the receive chain and provide enough attenuation at the proper frequencies to lower the power coupled into the LNA to acceptable levels. The level considered acceptable, however, is completely dependent on specifications of the hardware employed in a given system.

As a case study, consider the Thales Alenia RX09 line of satellite receivers. This includes receivers in both the C and Ku bands. For its C-band receiver, the maximum operating input power is listed as "15 dBm - Gain," where this gain is that of the LNA contained within and is specified to be within a range of 55-70 dB with a typical value of about 60 dB. Thus, the maximum input power can be considered to be -45 dBm. Many receivers also include an "overdrive" mode, with a higher maximum input power; the RX09 C-band receiver lists its overdrive input at 30 dBm - Gain, and says that the assembly can sustain this level for 2,000 hours without degradation or damage. If this level or time period is surpassed, however, permanent damage could be done to the receiver. Their Ku-band receiver is similar, and lists the same values for its maximum input powers. The catalog for the receivers also lists separate C-band and Ku-band LNAs with their own specifications. Their Ku-band LNA is rated for a maximum operating input power of -40 dBm and a maximum overdrive

of -20 dBm, while the C-band LNA is rated for a -40 dBm operating power and a -30 dBm overdrive.[3] As a second case study, Mitsubishi Electric also lists specifications for a C-band receiver, TMB-2015-48, and LNA, TMB-2015-055. The receiver lists an input level of -43 dBm, while the LNA lists a maximum input level of -64 dBm and an overdrive input level of -45 dBm for 24 hours.[2, 1]

Notably, all three receiver assemblies described here include a bandpass filter before the downconverter, but *after* the LNA. This means that all energy coupled into the receiver from a servicing satellite's transmitters would enter the LNA with little to no attenuation. And based on the peak coupling values found through the GRASP scenarios and summarized in Table 5.1, the input power from a nearby servicing satellite could exceed the maximum operating input power values for these receivers, and in some cases even the overdrive maximum input power. This places receivers built like these at extreme risk of damage when approached by another satellite.

5.3 Recommendations

Just because there is a risk of interference with and/or damage to a client does not mean that satellite servicing cannot be done safely. In fact, the analysis done to determine that there is a risk can also be used as a guide for how to mitigate it. The following is a list of recommendations of measures that can be taken by both clients and servicers in order to make servicing safer:

- The work done in this thesis examines the danger from RF coupling. Of course, if a servicing satellite did not use an RF communication system, this whole point would be moot. Optical communication is seeing much more use recently in space-based applications, and its high data rates and lack of interaction with RF components would make it a great candidate for use on a servicing satellite. Its drawbacks include the need for high pointing accuracy, which can be a challenge when there is a client to maneuver around, and the inability to communicate with a ground station when there is cloud cover. Still, if these challenges can be overcome, a servicing mission is an excellent application for

an optical communication system.

- If an RF system is used, all signs point to the fact that using a higher frequency band will result in better outcomes overall. The coupling is generally lower in higher frequencies, and the signals sent to the client from the ground in those bands will on average be stronger as well, giving them a greater chance of being received over the added noise from a servicer. Drawbacks of this include increased atmospheric and rain attenuation as the band is moved toward Ka-band, meaning higher transmit power on the servicer to compensate and therefore higher coupling.

- The part of the rendezvous with the highest level of coupling is the final approach from above. This is also the point in the CONOPS in which servicing satellite operators will want the greatest amount of telemetry, imagery, and video of the approach. Without efforts to reduce the effects of the increased transmissions on the client, these two situations are potentially incompatible. From a CONOPS perspective, to avoid transmitting at the most sensitive region, the servicer could try approaching the client from a different direction, although from an orbital mechanics and navigation standpoint this may be infeasible. Another possibility is holding all transmissions until the servicer is below the "danger zone" where the coupling peaks above the client, but this is also an unfavorable course of action, as the operators for both satellites will want to know very precise information about what the servicer is doing and where it is so that it does not cause other kinds of damage to the client. As such, other types of mitigation will likely need to be considered before these measures are taken seriously.

- As seen in many of the scenarios, polarization can have a great impact on the amount of power coupled into the receivers on the client. The polarizations used on the client should be well known to the servicer operators long before they begin to rendezvous, and a versatile servicer should have different polarizations available for use so it can utilize the ones that will interfere with a given client

the least.

- This thesis finds a tradeoff between using a highly directional antenna and one with a broader pattern. The directional one is generally more favorable as it leads to lower coupling in most cases, *unless a client's receiver happens to fall within its main beam.* A lower gain antenna does not have the risk of having a region with extremely high coupling, but it does have higher coupling overall in all other regions. The ideal way to perform a servicing mission with RF communications would be to employ a directional antenna and take extreme precautions to make sure the client's receivers stay out of its main beam. The data show that with the assumed parameters for the RSV, this is achieved when it gets to within about 40 m above the client. If it were to approach from a slight angle, rather than from directly above, all negative effects of coupling from its main beam can be avoided. In the same way, avoiding transmitting during the portions of the inspection phase when the servicer is directly above or beneath the client could go a long way in reducing the possibility of overwhelming coupling. These solutions are subject to what is possible under the guidance and navigation plan for the servicer, and would also need to be worked into the overall CONOPS, but stand a good chance at improving mission viability.

- Servicers should expect a similar amount of coupling from their clients, and should take all necessary precautions to ensure their receivers are protected and include proper filters such that only a signal in the appropriate band will be able to enter the receive chain and the LNA.

Many GEO satellite operators are waiting for initial demonstrations of on orbit servicing to make a judgment about the safety and practicality of the practice. Their satellites were not designed with servicing in mind, and as such satellites that do perform servicing operations will need to be extremely wary about how their clients are constructed. From an RF standpoint, this means taking a look at their receiver design and assessing the level of risk with applying external RF power sources to them. The initial servicing demonstration missions would do well to make sure that

their first clients are well protected. For future spacecraft launching into GEO, if they want to design their spacecraft to be serviced at some point in their mission lifetimes, they should ensure their receivers have filters in them to protect their most sensitive components. This is a small change that would go a long way towards increasing service life for clients and satellite servicing as a paradigm. This is simply one design change out of several that can be implemented to make future GEO spacecraft more robust and to make the job of a servicing spacecraft that much easier and less risky.

5.4 Conclusion

When examining the challenges associated with a satellite servicing mission, communications is an aspect that can be easy to overlook. So many other problems must be solved to ensure the success of the mission, such as navigation, RPO, docking, differential charge on the servicer and client, and others that it can be tempting to say that the servicer will use a different frequency than its client and call that good enough. However, as this thesis shows, even in different frequency bands enough power can be transmitted by a servicer that, in close enough proximity, it can couple into the receivers on the client and potentially interfere with the reception of its intended signals or damage receiver components if the power level is high enough. While this risk is very real, it is not a death sentence for satellite servicing, as there are things that can be done to prevent unwanted coupling, or at least reduce the amount of energy that is coupled. The risk is also highly dependent on the exact parameters of the communications systems on both satellites; this thesis makes a great deal of assumptions about what these look like, and tries to emulate planned missions using public information where possible, but a more detailed risk assessment can only be done with more complete knowledge about transmitter power levels, gain patterns, receiver schematics, and other parameters outlined above. What has been done here is that a case has been made that this is a concern that needs to be addressed just as much as any other servicing mission challenge. To make their operations safe for themselves and for their clients, servicing satellite operators should take heed of the

practices that increase and decrease unintended RF coupling in order to minimize the negative impact they have on other satellites while still delivering the many positive outcomes that a servicing mission can provide. This will allow the servicing industry to become more widely accepted and realize its full potential.

Bibliography

[1] C-band low noise amplifier. Datasheet. TMB-2015-055 Rev. A.

[2] C-band receiver. Datasheet. TMB-2015-048 Rev. A.

[3] Receiver - LNA - DOCON. Thales Alenia, May 2012. Satcom Components Catalog.

[4] MEV mission profile. `https://www.youtube.com/watch?v=d_DDmu-c5-Q`, 2017.

[5] AGI. STK Satellite CAD Model, 29 August 2006.

[6] Brian Berger and Jeff Foust. DARPA picks SSL as satellite-servicing partner despite Orbital ATK lawsuit. *SpaceNews*, 9 February 2017.

[7] David Calcutt and Laurie Tetley. *Satellite Communications: Principles & Applications.* Elsevier, Ltd., 1994.

[8] R. H. Clarke and John Brown. *Diffraction Theory and Antennas.* John Wiley & Sons, Inc., 1980.

[9] Stephen Clarke. Launch schedule. `https://spaceflightnow.com/launch-schedule/`, 2019. Spaceflight Now.

[10] eoPortal. ETS-VII (Engineering Test Satellite VII) / Kiku-7. `https://directory.eoportal.org/web/eoportal/satellite-missions/e/ets-vii`, 2002.

[11] Ho-Sung Choi et. al. Analysis of GEO spacecraft anomalies: Space weather relationships. *Space Weather*, Vol. 9.

[12] Northrop Grumman. Mission Extension Vehicle (MEV). Fact Sheet, 2018.

[13] Caleb Henry. MDA restarts satellite servicing business with SES as first customer, 2017.

[14] Caleb Henry. SSL cancels DARPA satellite servicer agreement, 30 January 2019.

[15] Frank Jensen. *Coupling add-on.* TICRA. GRASP Coupling Manual.

[16] Peter C Klanowski. Chronology of satellite failures. `http://www.sat-index.co.uk/failures/`, 2019. Satellite News Digest.

[17] John D. Kraus. *Antennas.* McGraw-Hill, Inc., second edition, 1988.

[18] Andrew Ogilvie, Justin Allport, Michael Hannah, and John Lymer. Autonomous satellite servicing using the orbital express demonstration manipulator system. Technical report, MDA, 9445 Airport Road, Brampton, Ontario, Canada L6S 4J3, June 2008.

[19] Benjamin Reed. Robotic refueling mission. `https://sspd.gsfc.nasa.gov/robotic_refueling_mission.html`, 2015. NASA Satellite Servicing Projects Division.

[20] Benjamin Reed. Robotic refueling mission - phase 2. `https://sspd.gsfc.nasa.gov/rrm_phase2.html#demonstrations`, 2015. NASA Satellite Servicing Projects Division.

[21] Benjamin Reed. RRM task overview. `https://sspd.gsfc.nasa.gov/rrm_tasks.html`, 2015. NASA Satellite Servicing Projects Division.

[22] Benjamin Reed. Restore-L satellite servicing mission. `https://sspd.gsfc.nasa.gov/restore-l.html`, 2018. NASA Satellite Servicing Projects Division.

[23] Benjamin Reed. RRM3. `https://sspd.gsfc.nasa.gov/RRM3.html`, 2018. NASA Satellite Servicing Projects Division.

[24] Gordon Roesler. Robotic servicing of geosynchronous satellites proposers day. Presentation, May 2016.

[25] Warren L. Stutzman and Gary A. Thiele. *Antenna Theory and Design.* John Wiley & Sons, Inc., second edition, 1998.

[26] Al Tadros, 11 January 2018. Phone interview.

[27] Hubregt J. Visser. *Array and Phased Array Antenna Basics.* John Wiley & Sons, Ltd., 2005.

[28] Thomas L. Wilson. Application for authority to launch and operate a mission extension vehicle. FCC technical narrative, Space Logistics, LLC, 24 February 2017.